



UNIVERSITY OF LEEDS

This is a repository copy of *Deposition of Inorganic Carbonate, Sulfate and Sulfide Scales on Anti-fouling Surfaces in Multiphase Flow*.

White Rose Research Online URL for this paper:  
<http://eprints.whiterose.ac.uk/121695/>

Version: Accepted Version

---

**Article:**

Keogh, W, Neville, A [orcid.org/0000-0002-6479-1871](https://orcid.org/0000-0002-6479-1871), Huggan, M [orcid.org/0000-0002-3297-4964](https://orcid.org/0000-0002-3297-4964) et al. (8 more authors) (2017) Deposition of Inorganic Carbonate, Sulfate and Sulfide Scales on Anti-fouling Surfaces in Multiphase Flow. *Energy and Fuels*, 31 (11). pp. 11838-11851. ISSN 0887-0624

<https://doi.org/10.1021/acs.energyfuels.7b02165>

---

© 2017 American Chemical Society. This document is the Accepted Manuscript version of a Published Work that appeared in final form in *Energy and Fuels*, copyright © American Chemical Society after peer review and technical editing by the publisher. To access the final edited and published work see <https://doi.org/10.1021/acs.energyfuels.7b02165>

**Reuse**

Items deposited in White Rose Research Online are protected by copyright, with all rights reserved unless indicated otherwise. They may be downloaded and/or printed for private study, or other acts as permitted by national copyright laws. The publisher or other rights holders may allow further reproduction and re-use of the full text version. This is indicated by the licence information on the White Rose Research Online record for the item.

**Takedown**

If you consider content in White Rose Research Online to be in breach of UK law, please notify us by emailing [eprints@whiterose.ac.uk](mailto:eprints@whiterose.ac.uk) including the URL of the record and the reason for the withdrawal request.



[eprints@whiterose.ac.uk](mailto:eprints@whiterose.ac.uk)  
<https://eprints.whiterose.ac.uk/>

1  
2  
3  
4  
5  
6  
7  
8  
9  
10  
11  
12  
13  
14  
15  
16  
17  
18  
19  
20  
21  
22  
23  
24  
25  
26  
27  
28  
29  
30  
31  
32  
33  
34  
35  
36  
37  
38  
39  
40  
41  
42  
43  
44  
45  
46  
47  
48  
49  
50  
51  
52  
53  
54  
55  
56  
57  
58  
59  
60

# Deposition of Inorganic Carbonate, Sulfate and Sulfide Scales on Anti-fouling Surfaces in Multiphase Flow

William Keogh,<sup>\*,†</sup> Anne Neville,<sup>†</sup> Michael Huggan,<sup>†</sup> Violette Eroini,<sup>‡</sup> John Helge Olsen,<sup>‡</sup> Frank Møller  
Nielsen,<sup>‡</sup> Salima Baraka-Lokmane,<sup>§</sup> Etienne Bourdelet,<sup>§</sup> Jon Arne Ellingsen,<sup>||</sup> Oeystein Bache,<sup>||</sup> and  
Thibaut Charpentier,<sup>Φ</sup>

<sup>†</sup>Institute of Functional Surfaces (iFS), University of Leeds, Leeds, LS2 9JT, England

<sup>‡</sup>Statoil ASA, 5020, Bergen, Norway

<sup>§</sup>TOTAL, 64000, Pau, France

<sup>||</sup>Conoco Phillips, 4056, Stavanger, Norway

<sup>Φ</sup>School of Chemical and Process Engineering (SCAPE), University of Leeds, Leeds, LS2 9JT, England

1  
2  
3  
4  
5  
6  
7  
8  
9  
10  
11  
12  
13  
14  
15  
16  
17  
18  
19  
20  
21  
22  
23  
24  
25  
26  
27  
28  
29  
30  
31  
32  
33  
34  
35  
36  
37  
38  
39  
40  
41  
42  
43  
44  
45  
46  
47  
48  
49  
50  
51  
52  
53  
54  
55  
56  
57  
58  
59  
60

**ABSTRACT:** Impairment of flow by way of mineral scale formation is a major complication affecting production in the oil and gas industry. Sour reservoirs contain hydrogen sulfide (H<sub>2</sub>S) that can prompt the formation of exotic metal sulfide scales, leading to detrimental fouling that can negatively impact production. The contrast in the mode of precipitation (solid formation from liquid solution) and deposition of both sulfide scale and conventional inorganic carbonate and sulfate scales is herein examined. Design of an experimental rig allowing diffusion of H<sub>2</sub>S gas into the brine phase of a sealed reaction vessel, resulted in a realistic representation of scaling processes occurring within sour reservoirs. Multiphase conditions, induced by introduction of a light oil phase to scaling brine within a turbulent regime, aimed to study the effect of oil and water wetting on pipeline fouling. Performance of a range of anti-fouling surfaces was determined through measurement of scale deposition by gravimetry and microscopy techniques. Under conditions modelled to reflect a typical H<sub>2</sub>S-containing reservoir, the contrasting scaling mechanisms of conventional calcium carbonate (CaCO<sub>3</sub>) and barium sulfate (BaSO<sub>4</sub>) scales when compared to lead sulfide (PbS) scale, highlighted the critical role of the light oil phase on deposition. Whilst conventional scales showed deposition by both crystallization and adhesion onto surfaces, the thermodynamic driving force for PbS prompted rapid bulk nucleation, with adhesion acting as the overwhelmingly dominant mechanism for deposition. The results showed that the addition of a 5% v/v light oil phase had a profound effect on scale particle behavior and deposition onto anti-fouling surfaces of varying wettability as a result of two processes. Primarily, the oil wetting of hydrophobic surfaces acted as a barrier to deposition; and secondly, adsorption of scale crystals at the oil/water interface of oil droplets within a turbulent oil-in-water emulsion, resulted in adhesion to hydrophilic surfaces after impaction. It is therefore proposed that sulfide scale, typically deposited in the upper regions of production tubing, is driven by adhesion after formation of a PbS solid-stabilized Pickering emulsion. This contrasts with the commonly held view that metal sulfides precipitate and deposit similarly to conventional scales, whereby salts crystallize both directly upon surfaces and in the aqueous bulk phase as solubility decreases towards the wellhead.

## 1. INTRODUCTION

The consideration of zinc sulfide (ZnS) and lead sulfide (PbS) as a significant flow assurance challenge within the oil and gas industry is a relatively recent development; publications aimed at its inhibition and removal have occurred only within the last two decades. Whilst previous mitigation studies incorporating surface science have focused primarily on researching anti-fouling surfaces to prevent more prevalent carbonate and sulfate scales 1-3, the complications in oil and gas production associated with deposition of sulfide scales are becoming increasingly frequent in high temperature/high pressure (HT/HP) systems. As such, greater emphasis is now being placed on understanding the fundamental mechanisms that drive sulfide scale formation and deposition; and exploring the potential of anti-fouling surfaces to offer a more affordable solution to mineral scaling, both in terms of capital and operating costs.

Much of the work available in the literature published investigating ZnS and PbS deposition details the chemical inhibition of such scales, based on the reaction of hydrolyzed hydrogen sulfide (H<sub>2</sub>S) derived from sodium sulfide (Na<sub>2</sub>S) and a metal cation, resulting in immediate homogeneous precipitation of all reactants within the bulk liquid phase <sup>4-6</sup>. The toxic and corrosive nature of H<sub>2</sub>S gas even at low concentrations and complications that arise as a result, likely account for the limited usage of gas in previous sulfide scaling experiments. In this study, a new method and apparatus whereby H<sub>2</sub>S gas introduced into the air-space of an anaerobic reaction vessel, gradually diffusing into the aqueous phase before reaching equilibrium and dissociating into reactive bisulfide species, is employed. The procedure more closely reflects mechanisms and conditions during production within a sour production well, where PVT studies have shown that aqueous H<sub>2</sub>S concentrations reach up to approximately 55 ppm at equilibrium; and turbulent, two-phase flow conditions are generated in an anaerobic environment <sup>7</sup>. Further experiments, contrasting the precipitation and deposition mechanisms of 'conventional' carbonate and sulfate scales onto anti-fouling surfaces, supplant current notions within the oil and gas industry that metal sulfides nucleate directly onto surfaces <sup>6, 8</sup>, instead highlighting the role of the light oil phase on homogeneous scale adhesion. The design and development of an airtight delivery vessel allowed

1 introduction of incompatible seawater and formation water brines under anaerobic conditions. Turbulence  
2 within the reaction vessel ensured that an oil in water (o/w) emulsion was created with the aqueous and  
3 light oil phase present within the system, modeling a multiphase flow within a production tubing line.  
4  
5  
6  
7  
8  
9

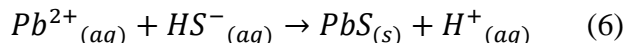
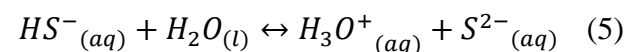
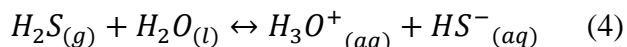
## 10 **2. BACKGROUND**

### 11 **2.1. Scale formation**

12  
13  
14  
15 Carbonate scales are common and have the ability to form and build-up rapidly upon surfaces <sup>9</sup>. Whilst  
16 the formation of barium sulfate (BaSO<sub>4</sub>) scale, like metal sulfides, is prompted by the injection of sulfate  
17 containing seawater, calcium carbonate (CaCO<sub>3</sub>) can precipitate during the primary recovery phase.  
18  
19

20  
21  
22 Lead and zinc sulfide scale deposits have become a concern in a number of North Sea oil and gas fields,  
23 rich in both evolved H<sub>2</sub>S gas and formation metal ions <sup>10</sup>. Sulfide ore deposits of lead (Pb<sup>2+</sup>) and zinc  
24 (Zn<sup>2+</sup>), known as Mississippi Valley Type (MVT) deposits, are commonly observed in Devonian to  
25 Permian and Cretaceous to Tertiary formations <sup>11</sup>. As a result, cations of lead and zinc are found naturally  
26 in many formation waters in HT/HP fields due to mineral dissolution of these ores over millions of years.  
27  
28

29  
30  
31  
32  
33  
34  
35  
36  
37  
38  
39  
40  
41  
42  
43  
44  
45  
46  
47  
48  
49  
50  
51  
52  
53  
54  
55  
56  
57  
58  
59  
60  
Dependent on pH, sulfide (S<sup>2-</sup>) and/or bi-sulfide (HS<sup>-</sup>) anions form when H<sub>2</sub>S gas present in the reservoir  
diffuses into formation water, and consequently dissociates. Anions are highly susceptible to precipitate  
into sulfide scales when reacted with aqueous metal cations such as Pb<sup>2+</sup> and Zn<sup>2+</sup>, present in formation  
waters <sup>12</sup>. Injected water used for pressure support can also enrich seawater with heavy metal ions from  
the formation <sup>13</sup>. Evolution of H<sub>2</sub>S gas within reservoirs can occur through both microbiological (souring)  
and geochemical means; a consequence of the increased activity of Sulfate Reducing Bacteria (SRB) and  
chemical reactions resulting from seawater injection, respectively <sup>14</sup>. The dissociation of H<sub>2</sub>S to its  
constituent anions in water can be seen in equations 4 and 5, with Pb<sup>2+</sup> cations within produced water  
reacting readily with sulfide based species to form PbS (galena), as seen in equation 6.



Concentrations of dissolved aqueous H<sub>2</sub>S in the produced water of North Sea oil wells have been recorded at levels as high as 55 ppm during production, yet it has been reported that concentrations as low as 2 ppm are sufficient to prompt formation of sulfide scale<sup>8,9</sup>. Whilst both PbS and ZnS scales are rarely found in isolation, this contribution focuses solely on PbS deposition to simply and effectively characterize the metal sulfide scaling mechanism, and highlight the contrast between sulfide and conventional scales. Precipitation of PbS crystals and the location at which they adhere to surfaces of production equipment or tubing is reported to be based upon changes in temperature, water chemistry, pH and residence time; in addition to the oil composition, characteristics and water-cut<sup>13</sup>. Cubic PbS crystals precipitated in the bulk phase have been reported to range from 20-100 nm, a result of the remarkably high initial saturation ratio (SR<sub>initial</sub>) and nucleation rate allowing formation of thermodynamically stable nanometric particles<sup>15,16</sup>.

## 2.2. Anti-fouling surfaces

Previous research in the area of sulfide mineral scale prevention has predominantly focused on chemical inhibition<sup>5,17,18</sup>, or physical removal through acid chemical treatment combined with mechanical methods<sup>9</sup>. As an alternative to batch injection or reactionary mechanical techniques, the use of anti-fouling coatings has been proposed as a way to drastically reduce the initial deposition and build-up of inorganic scales on surfaces<sup>19-21</sup>. This contribution investigates a number of proposed anti-fouling coatings with diverse physio-chemical parameters, variants of which are already implemented in downhole applications due to their high durability and fouling resistant properties. The wettability of anti-scaling surfaces, particularly in multiphase conditions, has been shown to be of particular importance with regards to the degree of inorganic scales deposited<sup>22</sup>. Table 1 lists the name and type of coatings evaluated within this study, as

well as their general characteristics. Coatings F1, F2 and F3 are classed as hydrophobic (water contact angle over 90°) and the remainder hydrophilic (water contact angle below 90°).

Coating	Coating type
F1	Fluoropolymer
F2	
F3	
F4	
SG1	Sol-Gel
SG2	
SG3	
DLC	Diamond-like carbon
REF	UNS N07718 (none)

**Table 1** Anti-fouling coatings and coating type

### 2.3. Particle behavior at the o/w interface

Sub-micron sized particles are prone to being trapped at interfaces between water/oil fluid phases, with the degree of attachment to the interface partly determined by both size and the resulting three-phase contact angle of a given particle as a result of particle-particle, particle-oil and particle-water interactions<sup>23</sup>. A particle has different contact angle characteristics based on its wettability at the oil/water interface, with hydrophilic or hydrophobic surfaces having a contact angle smaller or larger than 90° respectively, as represented in Figure 1.

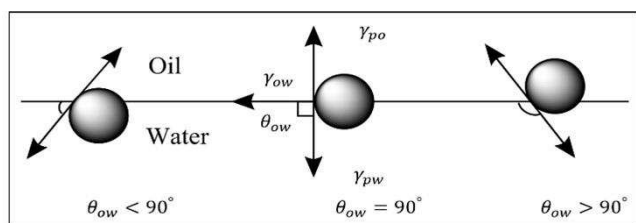


**Figure 1** Position of a solid particle at an o/w interface

Solid colloidal particles adsorb at the oil/water interface, after precipitation within the aqueous phase, through partial wetting of the solid by both phases. High resistance to coalescence of stabilized droplets results in the formation of a ‘Pickering emulsion’, whereby an emulsion of any type, either o/w, water-in-oil (w/o), or multiple, is stabilized by solid particles<sup>24</sup>, as illustrated in Figure 2.

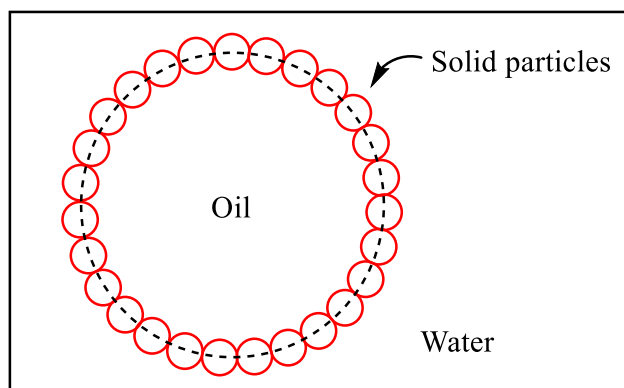


**Figure 2** Solid particles stabilized at the interface in an o/w Pickering emulsion

Stability of a Pickering emulsion is ultimately based on the dielectric discontinuity between water and oil; overall particle charge; particle wettability as a function of both composition and size; and the effect of particle diameter on average droplet size and emulsion stability<sup>24, 25-27</sup>.

### 3. EXPERIMENTAL METHOD

#### 3.1. Brine composition

Simple carbonate, sulfate and sulfide scaling brines were formulated in distilled water. Brine compositions and  $SR_{\text{initial}}$  values are presented in Tables 2-7.  $SR$  of  $\text{CaCO}_3$  is defined in equation 7:

$$SR = \frac{(IAP \text{ Ca})(IAP \text{ CO}_3)}{(K_{sp} \text{ CaCO}_3)} \quad (7)$$

Where  $IAP$  is ion activity product and  $K_{sp}$  is the solubility product of the scale forming species<sup>28</sup>.

Ion	Ionic concentration (mg/L)	
	Formation water	Sea water
$\text{Na}^+$	10000	11744
$\text{Ca}^{2+}$	8000	-
$\text{K}^+$	468	-
$\text{Mg}^{2+}$	1118	-
$\text{HCO}_3^-$	-	6102
$\text{Cl}^-$	36629	

**Table 2** Carbonate scaling brine composition

Salt	$SR_{\text{initial}}$
$\text{CaCO}_3$	76

**Table 3** Carbonate brine  $SR_{\text{initial}}$  at 20°C

Ion	Ionic concentration (mg/L)	
	Formation water	Sea water
Na <sup>+</sup>	31275	10890
Ca <sup>2+</sup>	2000	428
K <sup>+</sup>	654	1368
Mg <sup>2+</sup>	739	460
Ba <sup>2+</sup>	268	-
Sr <sup>2+</sup>	771	-
SO <sub>4</sub> <sup>2-</sup>	-	2960
Cl <sup>-</sup>	74306	

**Table 4** Sulfate scaling brine composition

Salt	SR <sub>initial</sub>
BaSO <sub>4</sub>	1888
SrSO <sub>4</sub>	4

**Table 5** Sulfate brine SR<sub>initial</sub> at 20°C

Ion	Ionic concentration (mg/L)	
	Initial brine	At equilibrium
Pb <sup>2+</sup>	1860	<1860
Cl <sup>-</sup>	640	640
H <sub>2</sub> S <sub>(aq)</sub>	0	30

**Table 6** PbS scaling brine composition

Salt	SR <sub>initial</sub>
PbS	2.8x10 <sup>22</sup>

**Table 7** PbS brine SR<sub>initial</sub> at 20°C

### 3.2. Experimental set-up

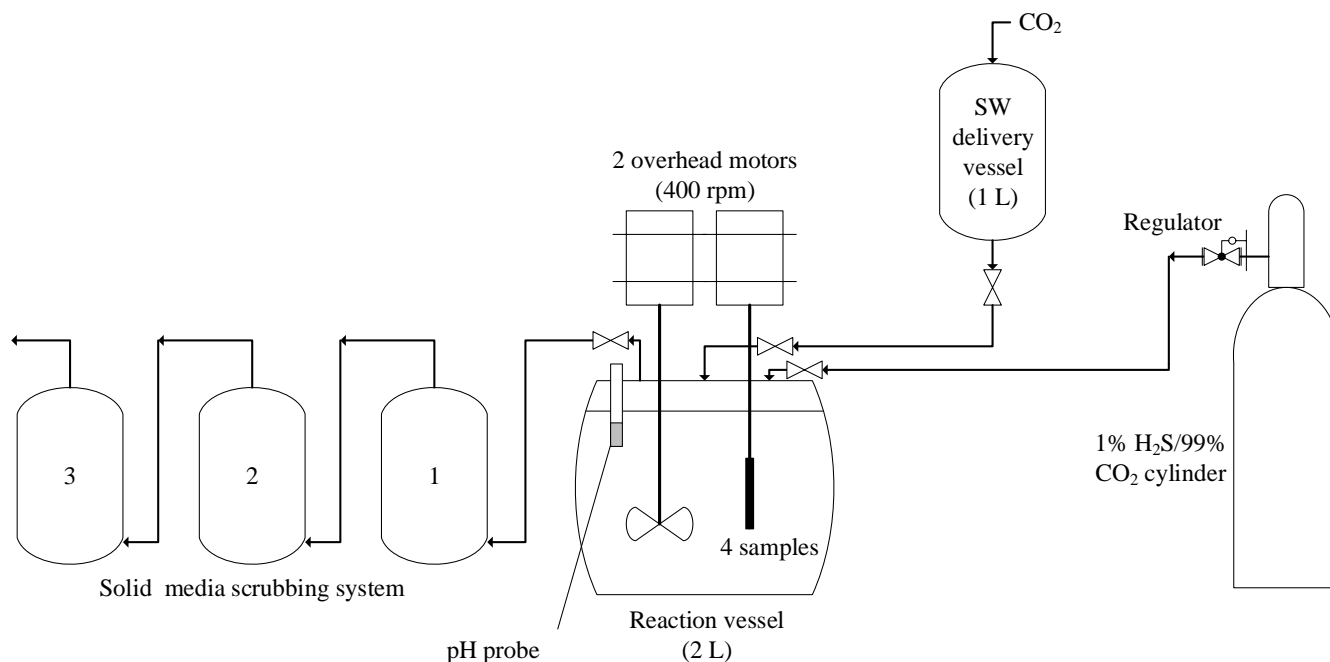


**Figure 3** Schematic diagram of experimental scaling rig

Figure 3 shows a schematic of the equipment, whereby a gas blend of 1% H<sub>2</sub>S/99% CO<sub>2</sub> or 100% CO<sub>2</sub> entered a 2 liter (L) reaction vessel under anaerobic conditions. Fed into the gaseous phase, H<sub>2</sub>S and CO<sub>2</sub> diffuse into the brine and subsequently dissociate/become hydrolyzed respectively. A bladed impeller connected to an overhead motor emulsified the oil and water phases in multiphase tests, with 4 samples (surface area of 3.77 cm<sup>2</sup> each) correspondingly rotated to create turbulence at the coating interface. Excess gas is fed into an activated carbon/alumina scrubbing system to remove H<sub>2</sub>S from the flow stream.

### 3.3. CaCO<sub>3</sub> and BaSO<sub>4</sub> scaling tests

For both carbonate and sulfate experiments, mineral forming formation water (FW) and seawater (SW) brines were mixed in a 1:1 ratio within the 2 L reaction vessel. Experiments performed under multiphase conditions introduced light synthetic distillate (C<sub>11</sub>-C<sub>16</sub> iso-alkanes) as the oil phase at a brine to oil ratio of 95:5 (v/v). Four cylindrical coupon samples were mounted upon the shaft and inserted into the vessel,

1 alongside a bladed impeller, with both rotated at 400 rpm by overhead stirrers. CO<sub>2</sub> gas was bubbled  
2 through the SW delivery vessel and the FW brine containing reaction vessel for one hour, ensuring  
3 anaerobic conditions in both incompatible brines before mixing, and was continuously fed into the reaction  
4 vessel throughout the experiment. Overpressure within the delivery vessel allowed flow of SW brine into  
5 the FW brine containing reaction vessel once a connecting valve was opened, initiating the experiment,  
6 before the valve was closed. The experiment run-time was 1 hour, after which the flow of CO<sub>2</sub> was stopped  
7 and the anti-fouling coupons carefully extracted. Sample were then dried in a 60°C oven for a 24 hour  
8 period to evaporate excess water and oil on the coating surface, allowing any mineral deposits to dry.  
9  
10  
11  
12  
13  
14  
15  
16  
17  
18  
19  
20  
21

### 22 3.4. PbS scaling tests

23 A lead (II) chloride (PbCl<sub>2</sub>) brine was formulated and stirred thoroughly for 1 hour in 2 L of distilled water  
24 to fully dissolve the PbCl<sub>2</sub> salt. Tests were run within an airtight reaction vessel, initially sparged with  
25 carbon dioxide (CO<sub>2</sub>) gas for a period of 2 hours to ensure anaerobic conditions during testing, preventing  
26 the formation of sulfates and the escape of H<sub>2</sub>S gas. Tables 6 and 7 show the brine composition and SR<sub>initial</sub>  
27 for PbS scaling experiments. 50 mL of acetic acid buffer (48 mL 5M acetic acid and 452 mL of 5M sodium  
28 acetate in 1 L distilled water) was used to make up the PbCl<sub>2</sub> brine, and maintained a constant pH of 5.2  
29 within the reaction vessel, determined by pH probe.  
30  
31  
32  
33  
34  
35  
36  
37  
38  
39  
40

41 Tests performed in a single phase consisted of 2 L of PbCl<sub>2</sub> brine; whilst multiphase experiments used  
42 PbCl<sub>2</sub> brine and synthetic light distillate, in a brine to oil ratio of 95:5 (v/v) made up to 2 L. Gas in a blend  
43 of 1% H<sub>2</sub>S/99% CO<sub>2</sub> was introduced into the air phase of the airtight reaction vessel at a constant pressure  
44 of 1.1-1.2 bar (absolute), controlled via a regulator connected to a pressurized cylinder (Figure 3). Under  
45 these conditions, the H<sub>2</sub>S concentration reached approximately 30 ppm in the aqueous phase at  
46 equilibrium, representative of concentrations recorded topside in sour North Sea brines <sup>8</sup>. Due to the  
47 toxicity of H<sub>2</sub>S gas, all experiments were carried out in a leak tested reaction vessel, with a series of three  
48 activated carbon/alumina based scrubbing systems, each 1 L in volume, to chemically adsorb unreacted  
49  
50  
51  
52  
53  
54  
55  
56  
57  
58  
59  
60

H<sub>2</sub>S gas. Post-experiment, the H<sub>2</sub>S/CO<sub>2</sub> stream was stopped and the system flushed with nitrogen (N<sub>2</sub>) to fully remove H<sub>2</sub>S within the reaction vessel and feed lines into the scrubbers. As in CaCO<sub>3</sub> and BaSO<sub>4</sub> scaling experiments, sample coupons were removed and dried in a 60°C oven for a 24 hour period.

A Malvern Bohlin Gemini rheometer with cone and plate geometry of CP 1°/40mm measured the viscosity of the formed PbS Pickering emulsion across a range of shears from 0.01 Pa to 2 Pa at 20°C.

### 3.5. Hydrodynamic conditions

A bladed impeller was rotated at 400 rpm, necessary to create an emulsion within the reaction vessel when synthetic distillate was present. To propagate turbulence at the surface of the anti-fouling coupons, the shaft was rotated at 400 rpm, with hydrodynamic conditions represented in Table 8 representative of flow conditions within a single phase system. Rotating cylinder (RC) equipment, used extensively in corrosion and scaling research was implemented as flow becomes turbulent at very low rotational velocities, with ( $Re > 300$ ) sufficient to create turbulence at the coupon surfaces<sup>29</sup>.

Parameter	Value
Reynolds number (Re)	3374
Wall shear stress $\tau$ (Pa)	0.17
Surface velocity $U_{cyl}$ (cm.s <sup>-1</sup> )	25.13

**Table 8** Hydrodynamic conditions at interface

### 3.6. Pre-precipitated PbS scaling tests

After PbS multiphase experiments in the presence of synthetic light distillate, new anti-fouling coupons of the same type (REF; F1; F2; SG2) were attached to the mounting shaft, inserted into the system, and the experiment re-run in the pre-precipitated, post-experimental brine. All other parameters were kept identical, allowing the degree to which the adhesion mechanism of bulk precipitated PbS particles onto surfaces was pre-dominant to be established.

## 4. RESULTS

### 4.1. CaCO<sub>3</sub> deposition in single phase flow

Calcite crystals can be seen to precipitate heterogeneously upon anti-fouling surfaces, characterized by clearly defined cubic and rhombohedral morphologies up to 20 microns ( $\mu$ ) in diameter, and x-ray diffraction (XRD). Limited secondary nucleation occurs upon calcite crystals, with further growth characterized by poorly defined, soft-edged CaCO<sub>3</sub>. From SEM images in Figure 5, and EDX analysis, it is clear that larger halite (NaCl) crystal deposits act as nucleation sites for secondary calcite precipitation, incorporating into the lattice based on the well-defined cubic growth.

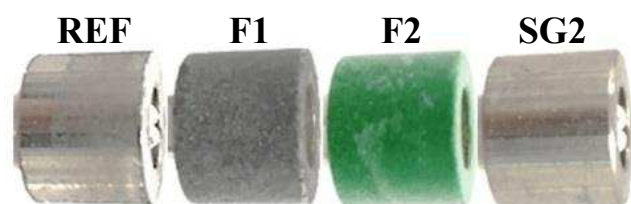


**Figure 4** Photographs of samples – CaCO<sub>3</sub> single phase conditions

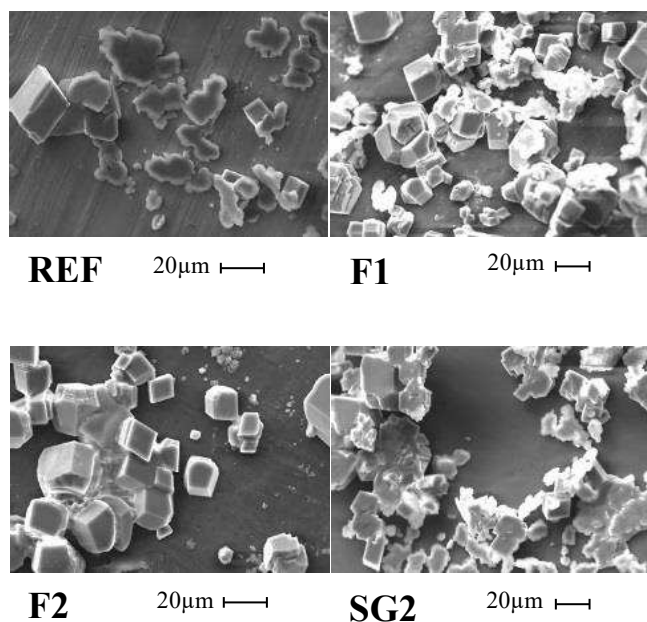


**Figure 5** SEM images – CaCO<sub>3</sub> single phase conditions

From Figure 6, it can be seen there is no correlation ( $R^2 = 0.1866$ ) between water contact angle and mass gain upon surfaces, with fluoropolymer surfaces showing a marginally higher degree of surface scaling. Fluoropolymers tend to have rougher surfaces as a consequence of application and finishing procedures, providing a high number of nucleation sites, resulting in higher surface scale coverage in single phase systems. This can be seen in work by Charpentier et al.<sup>21</sup>, where fluoropolymer surfaces undergo significant scaling in turbulent, single phase carbonate and sulfate systems.

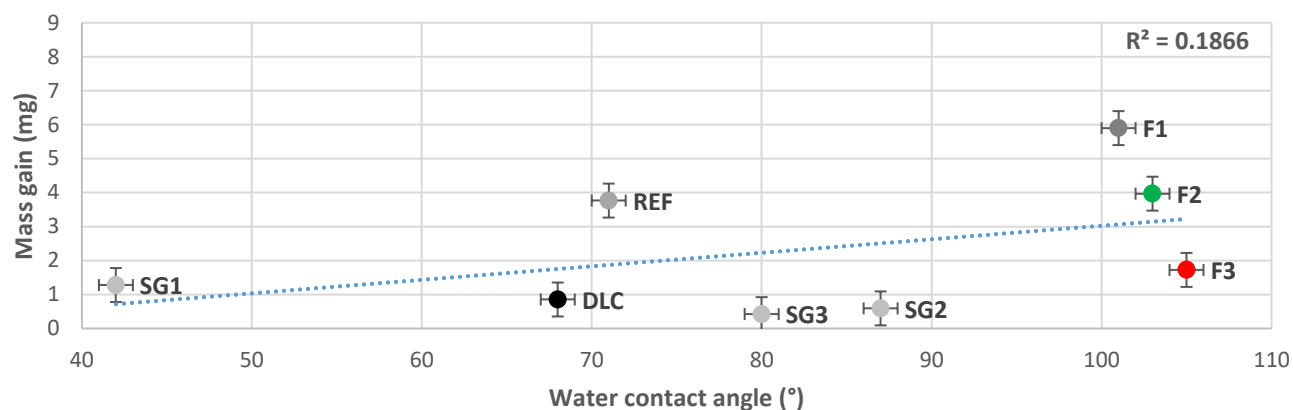
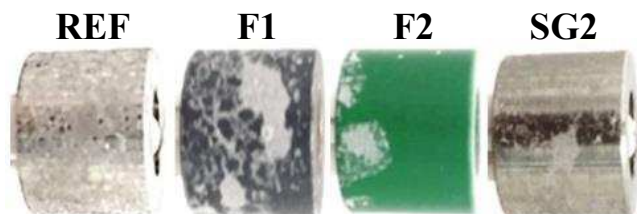


**Figure 6** Water contact angle vs. mass gain –  $\text{CaCO}_3$  single phase conditions

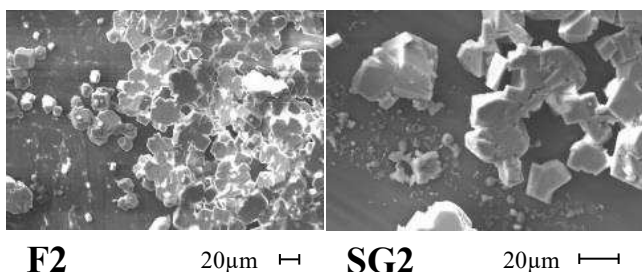
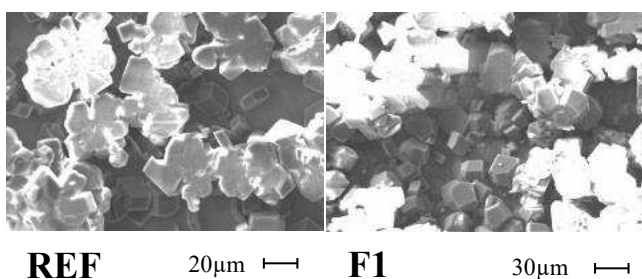
#### 4.2. $\text{CaCO}_3$ deposition in multiphase flow

Introduction of a light oil phase at 5% v/v to a carbonate scaling brine prompted increased deposition upon all samples where localized crystallization had occurred, with heterogeneously precipitated calcite acting as nucleation sites. Secondary nucleation and growth was more extensive than in single phase, demonstrated through comparison of scaling on REF coupons in Figures 5 and 8, where well-defined calcite crystals at the surface are overlain by large undefined calcite growths. This trend, replicated on other anti-fouling surfaces, can be explained by enhanced attraction between oppositely charged ions near the oil/water interface relative to that of the bulk, and the interface providing a thermodynamically favorable nucleation barrier for calcite precipitation<sup>30,31</sup>. Agglomeration of ionic clusters and calcite of

1 pre-critical radii at the oil/water interface in multiphase systems increases the mass of conglomerates and  
2 therefore kinetic energy of collision; a similar phenomenon to that seen in single phase, whereby growth  
3 rate of crystals as a result of secondary nucleation has been shown to increase with rising shear rate <sup>32, 33</sup>.  
4  
5  
6  
7  
8



17 **Figure 7** Photographs of samples – CaCO<sub>3</sub>  
18 multiphase conditions  
19



45 **Figure 8** SEM images – CaCO<sub>3</sub> multiphase  
46 conditions  
47  
48  
49

50 From Figure 9, the influence of presence of a light oil phase on depositional mass gain led to reversal  
51 of the trend seen in single phase CaCO<sub>3</sub> systems, though correlation was still very weak ( $R^2 = 0.1906$ ).  
52 Envelopment of the oil phase around fluoropolymer coatings reduced overall surface coverage of scale,  
53 an example of isolated nucleation seen on coupon F2 in Figure 7. Whilst scaling was for the most part  
54  
55  
56  
57  
58  
59  
60

prevented upon the F2 coupon surface, it is possible that imperfections act as nucleation sites, prompting heterogeneous nucleation that then culminates in an exponentially increasing rate of secondary nucleation confined to one site.

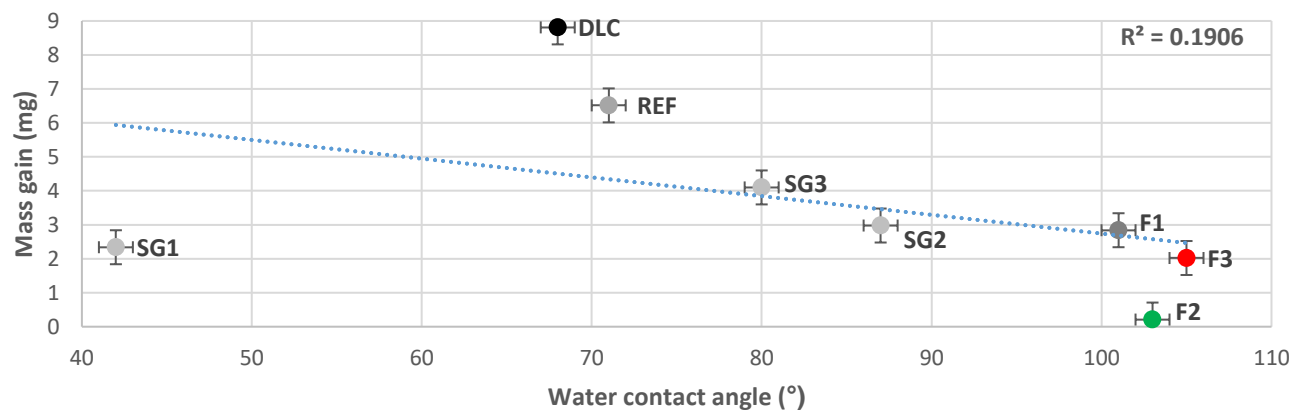


**Figure 9** Water contact angle vs. mass gain – CaCO<sub>3</sub> multiphase conditions

#### 4.3. BaSO<sub>4</sub> deposition in single phase flow

Determined from EDX, species of barite and orthorhombic strontium sulfate (SrSO<sub>4</sub>) can be seen to precipitate heterogeneously upon the surface at approximately 1 μm diameter in size, with surface coverage close to 100% in single phase systems. The high SR<sub>initial</sub> of BaSO<sub>4</sub> compared to CaCO<sub>3</sub> (1888 and 76 respectively) resulted in smaller stable crystal size and a higher degree of homogeneous nucleation and adhesion. Clustered, homogeneously precipitated BaSO<sub>4</sub> and SrSO<sub>4</sub> of snowflake-like appearance are visible upon REF, F1 and F2 coupons of Figure 11.

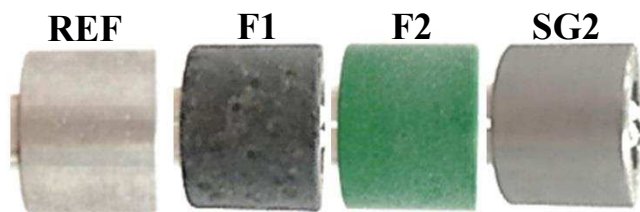


**Figure 10** Photographs of samples – BaSO<sub>4</sub> single phase conditions

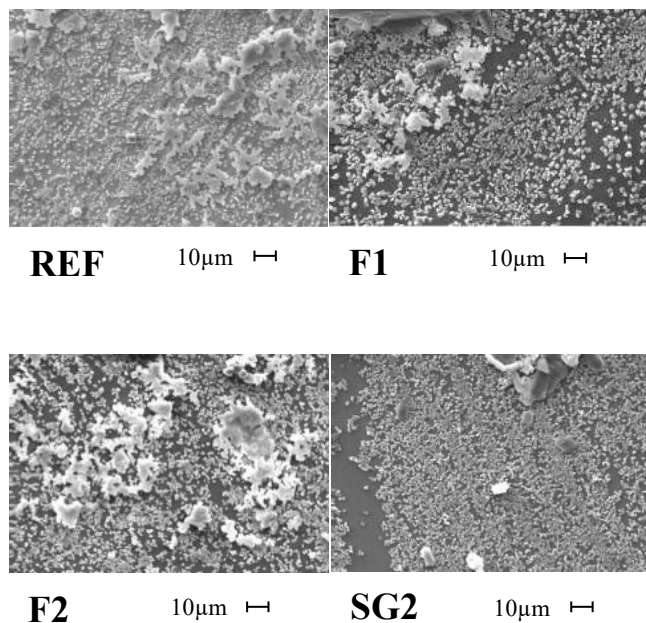


**Figure 11** SEM images – BaSO<sub>4</sub> single phase conditions

From Figure 12, there is no real correlation between coating water contact angle and mass gain ( $R^2 = 0.1234$ ). All surfaces show near total surface coverage, though due to small crystal size the mass gain seen on surfaces is comparatively lower than with CaCO<sub>3</sub> deposits.

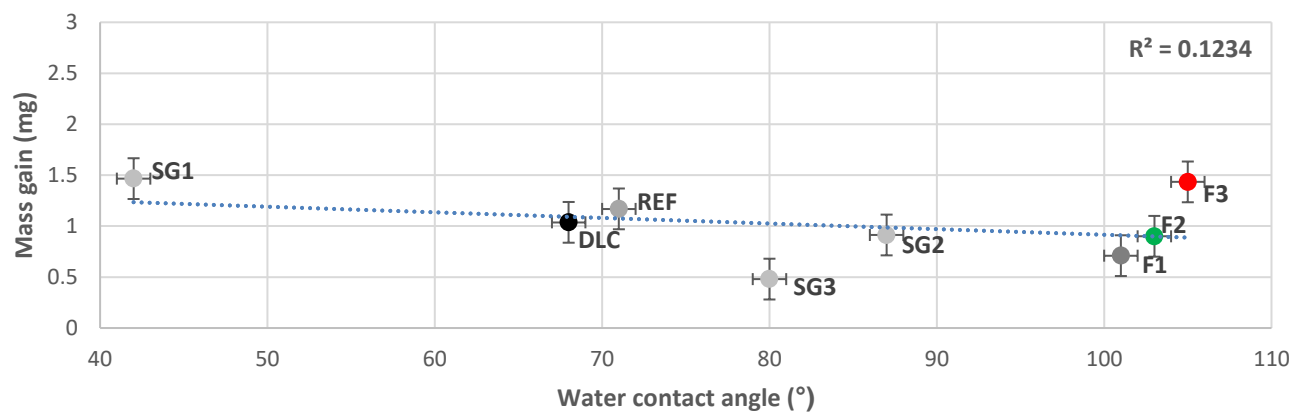


**Figure 12** Water contact angle vs. mass gain – BaSO<sub>4</sub> single phase conditions

#### 4.4. BaSO<sub>4</sub> deposition in multiphase flow

In multiphase sulfate systems, in terms of the depositional pattern of scale on coupons in Figure 13, a similar trend arose to that observed with carbonate scale. Hydrophilic surfaces (REF; SG2) showed uniform scale coverage, with circular areas visibly free of scale where oil droplets had impacted the surface. Hydrophobic surfaces (F1; F2) however, had isolated regions where deposition had occurred; with homogeneously precipitated scale adsorbed at the oil/water interface building up and adhering on to pre-scaled areas through collision of BaSO<sub>4</sub> and SrSO<sub>4</sub> scale particle-encapsulated oil droplets. Figure 14 shows SEM images of homogeneously precipitated ‘snowflake’ shaped deposits that have precipitated homogeneously within the bulk phase before depositing on the surface under the turbulent flow regime at the sample interface. EDX imaging showed that barite was the dominant crystal species present, with SrSO<sub>4</sub> interspersed throughout deposits on all surfaces.

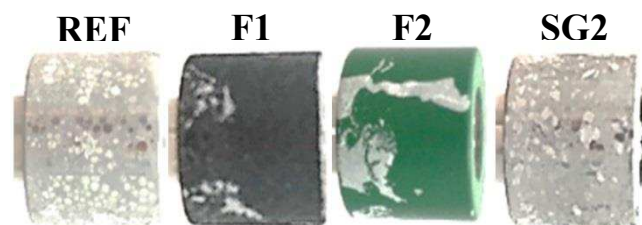


**Figure 13** Photographs of samples – BaSO<sub>4</sub> multiphase conditions

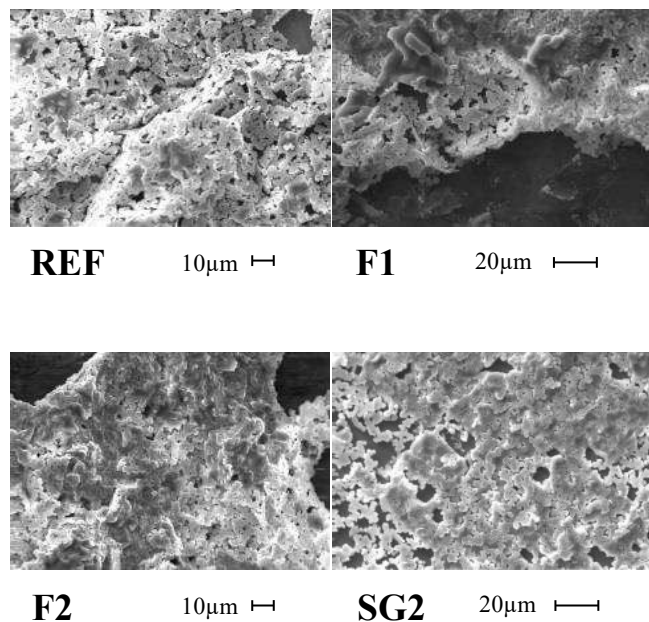


**Figure 14** SEM images – BaSO<sub>4</sub> multiphase conditions

A more definitive correlation ( $R^2 = 0.4186$ ) was observed for water contact angle vs. mass gain in sulfate systems (Figure 15), than when compared to a CaCO<sub>3</sub> based multiphase system (Figure 9); with fluoropolymers showing less mass gain in general than hydrophilic surfaces. The higher the  $SR_{initial}$  of a mineral salt, the more probable it is that stable crystal nuclei will precipitate homogeneously within the bulk phase<sup>34</sup>. The mass gain on surfaces through adhesion of scale particles from within the bulk phase is more heavily influenced by the presence of a light oil phase than those that nucleate directly for two reasons. Firstly, fluoropolymer surfaces are wetted by oil within an o/w emulsion as a result of their hydrophobicity, forming an enveloping layer that shields the surface from scale within the brine phase. Secondly, the adsorption of particles at the o/w interface of oil droplets (given that the particle is partially wetted) increases transport and deposition of homogeneously precipitated scale onto surfaces via droplet impaction. Due to the lack of an enveloping oil layer on hydrophilic surfaces, they are more prone to adhesion of partially-wetted particles under a turbulent regime.

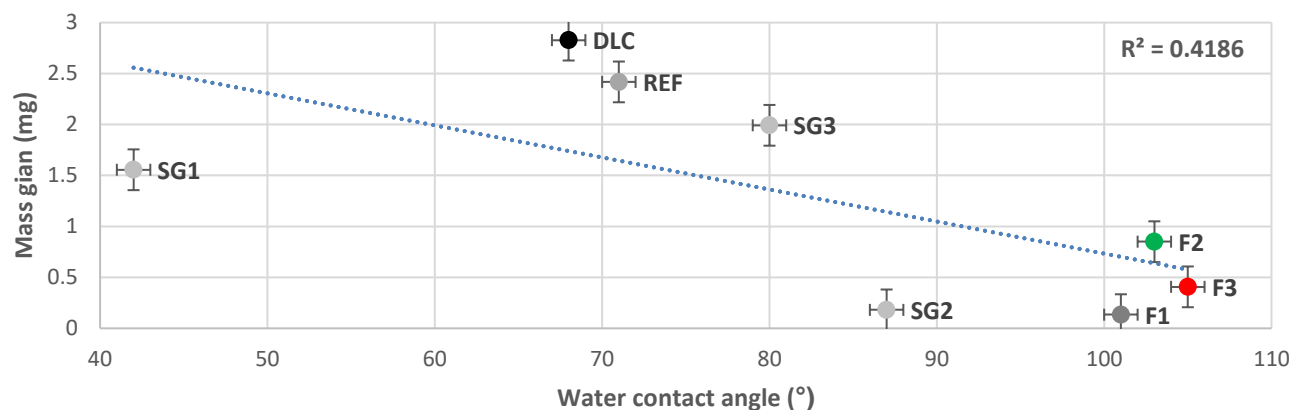
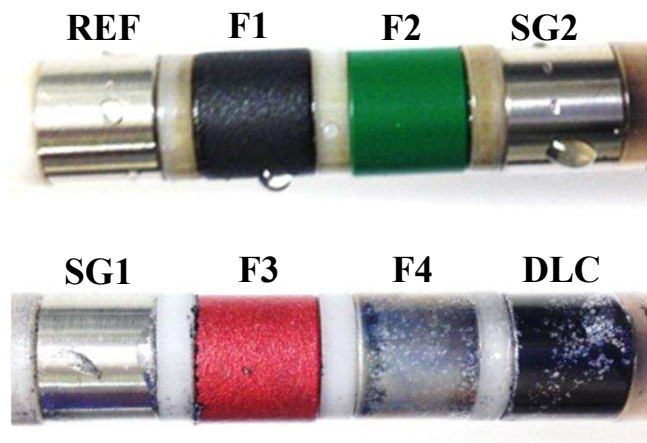


**Figure 15** Water contact angle vs. mass gain – BaSO<sub>4</sub> multiphase conditions

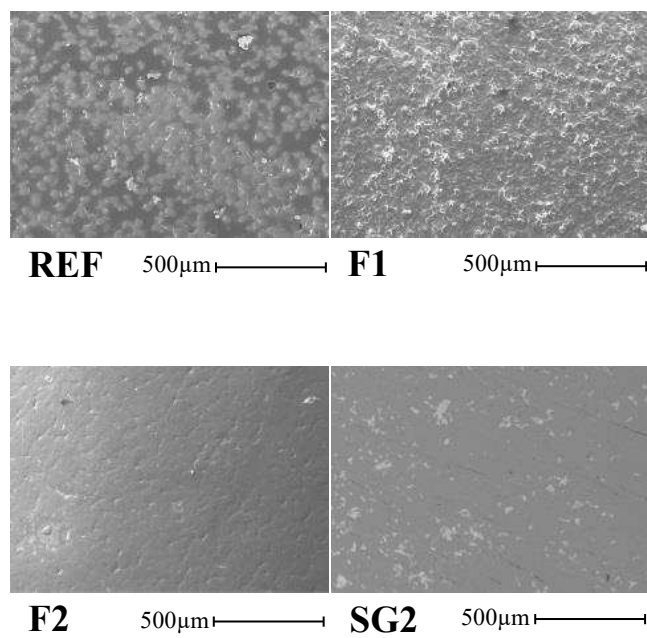
#### 4.5. PbS deposition in single phase flow

As a consequence of the exceedingly high  $SR_{\text{initial}}$  of  $2.8 \times 10^{22}$  for PbS in the system, scale precipitation occurred spontaneously within the homogeneous phase, with the rate-limiting step the gradual absorption into the aqueous phase and consequent dissociation of H<sub>2</sub>S to form aqueous HS<sup>-</sup> anions. The rate of PbS precipitation can be gauged through the darkening of the reaction solution over the course of the experimental run time, becoming an opaque black color after approximately 15 minutes over the course of 1 hour. Any homogeneously precipitated scale that therefore deposited onto a surface, did so by way of adhesion as opposed to heterogeneous precipitation, with agglomerates attaching to surfaces through turbulent and gravitational deposition. Loose deposits of PbS particles formed through aggregation of individual particles within the bulk phase, are associated with low adhesion rates to the surface. Agglomerates show increased detachment rates due to turbulence and high shear, where the dimensionless Reynolds number ( $Re$ ) is 3374 at rotary speeds of 400 rpm<sup>35</sup>. Figure 16 displays images of the anti-fouling coatings after removal from the reaction vessel post-experiment, with negligible PbS deposition on all surfaces, as seen on SEM images in Figures 17 and 18.



15  
16  
17  
18  
19

**Figure 16** Photographs of samples – PbS single phase conditions



44  
45  
46  
47  
48  
49  
50  
51  
52  
53  
54  
55  
56  
57  
58  
59  
60

**Figure 17** SEM images – PbS single phase conditions

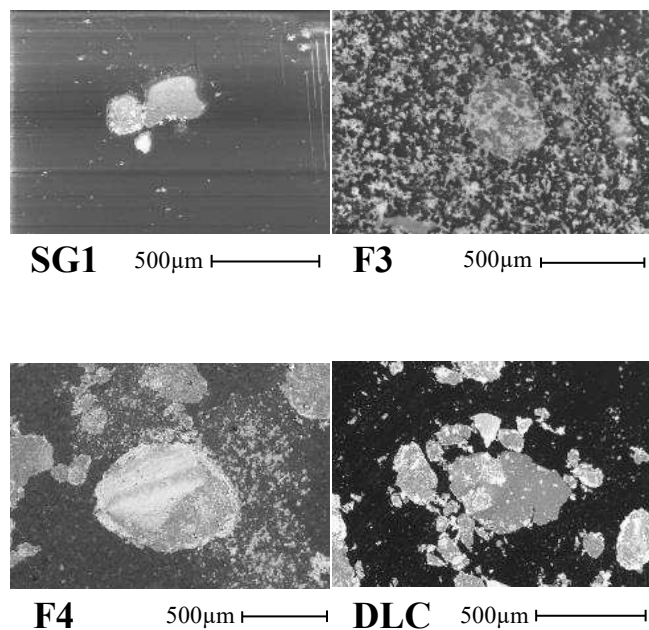


**Figure 18** SEM images – PbS single phase conditions

From Figure 19 it can be seen there is no correlation between mass gain and wetting properties of the anti-fouling surfaces, with very little deposition seen on surfaces. As deposition within the PbS precipitating system is adhesion driven, surface wettability has significantly less influence in a single phase system due to the low adherence of loose agglomerates; with topographical parameters such as roughness ( $R_a$ ) and kurtosis ( $R_{ku}$ ) likely to have greater significance. Work by Charpentier et al.<sup>21</sup> shows that whilst turbulent flow conditions on a surface significantly increase scale build-up in precipitating carbonate and sulfate systems, primarily due to the increased transport and availability of solute ion embryos at the sample surface and heterogeneous crystal interface; anti-fouling surfaces immersed in pre-precipitated carbonate and sulfate scaling brines under identical flow conditions show comparably negligible mass gain. Additionally, when adhesion of particles precipitated in the bulk phase is the sole mechanism for deposition, it has been shown that laminar flow ( $Re < 300$ ) results in higher surface mass gain due to a reduction of the critical shear stress required for removal of loose agglomerates at the adhering surface<sup>21</sup>.

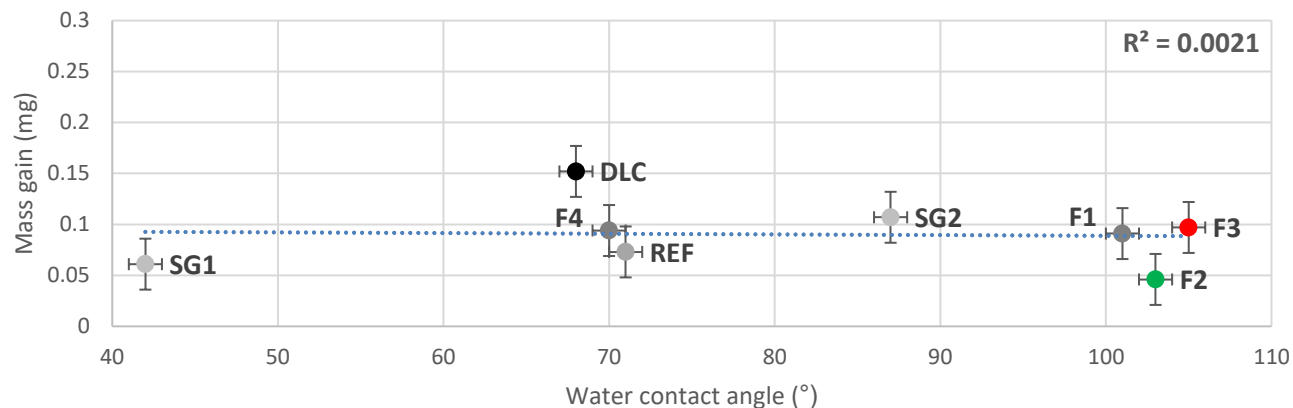


**Figure 19** Water contact angle vs. mass gain – PbS single phase conditions

Figure 20 shows the post-experimental brine, with loose PbS agglomerates formed within the bulk phase settling at the bottom of the vial. Surface energy of particles is reduced through agglomeration of nanometrically sized PbS particles, based on attractive van der Waals (VDW) and repulsive electrostatic interactions; and as a consequence, the settling of formed clusters is driven by gravitational deposition<sup>28</sup>.

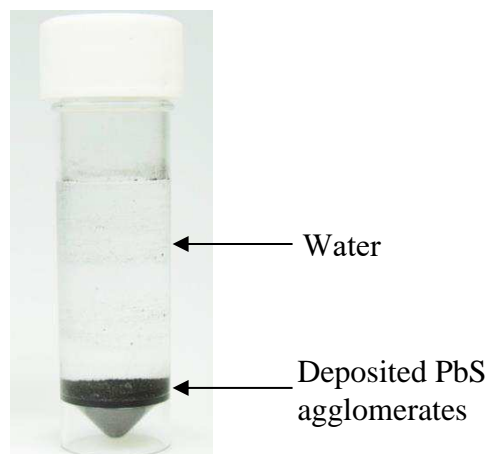


**Figure 20** Post-experiment – PbS single phase conditions

#### 4.6. PbS deposition in multiphase flow

As in single phase systems, homogeneous precipitation of PbS scale within the bulk phase of the system occurs spontaneously, with the rate-limiting step the diffusion and dissociation of H<sub>2</sub>S to form reactive HS<sup>-</sup> anions, as seen in equation 4. As such, darkening of the solution occurs at a similar rate to that seen in single phase, turning an opaque black color after approximately 15 minutes. pH measurements showed that the presence of an artificial oil phase at an brine to oil ratio of 95:5 (v/v) did not affect the pH of the solution, which was recorded at pH 5.2. Consequently, the SR<sub>initial</sub> of PbS and the rate of hydrolysis of H<sub>2</sub>S into the brine phase was unchanged. Additionally, as in a single phase system, adhesion was the sole mechanism driving the deposition of PbS scale. It can be seen from Figure 21 that a thick, black deposit has adhered to all anti-fouling surfaces, with the exception of fluoropolymer coatings F1, F2 and F3. The behavior of PbS particles changes dramatically with the addition of a light oil phase, with adsorption of PbS at the o/w interface under turbulent conditions, whereby oil droplets within the water phase are encapsulated and stabilized by solid nanoparticles. As a result, PbS particles anchored at the o/w droplet interface become adherent upon impaction of surfaces, forming circular deposits around the point of collision; as seen in Figures 22 and 23 on hydrophilic REF, SG2, SG1, F4 and DLC surfaces.

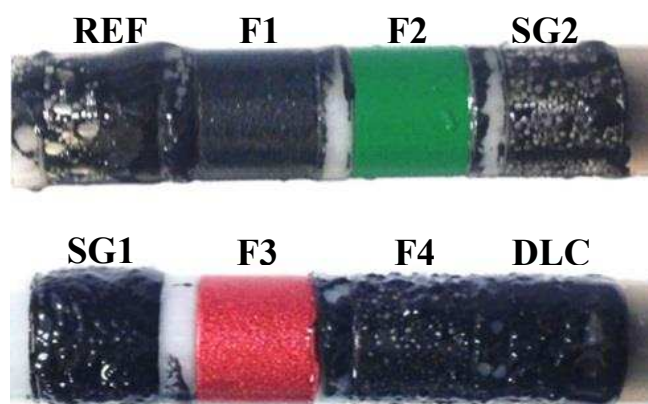
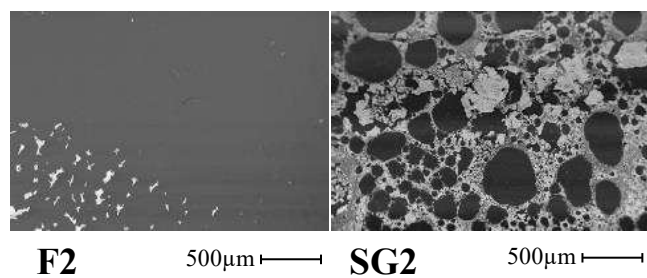
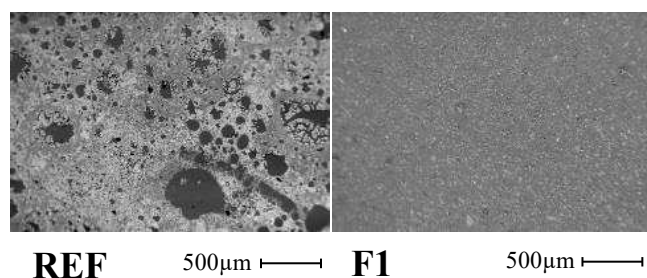
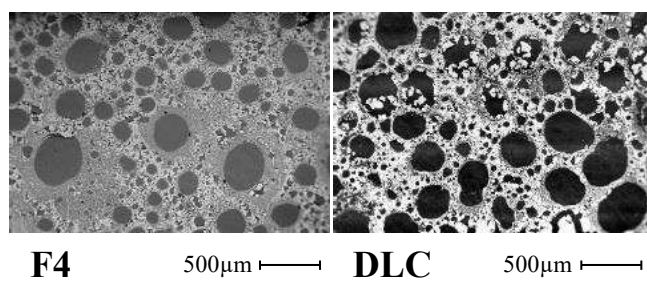
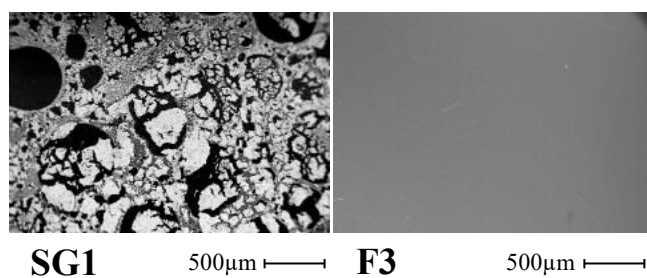


**Figure 21** Photographs of samples – PbS multiphase conditions



22 **Figure 22** SEM images – PbS multiphase  
23 conditions  
24



51 **Figure 23** SEM images – PbS multiphase  
52 conditions  
53

From Figure 24 it can be observed that there is a strong negative correlation between the water contact angle of an anti-fouling surface and the degree of mass gain through PbS scale deposition. Hydrophilic surfaces with a low contact angle see significant scale build-up, with the degree of PbS deposition decreasing as water contact angle increases. Coatings with a water contact angle over 90° that can be described as hydrophobic, such as fluoropolymer samples F1, F2 and F3, show little to no PbS deposition upon their surface.

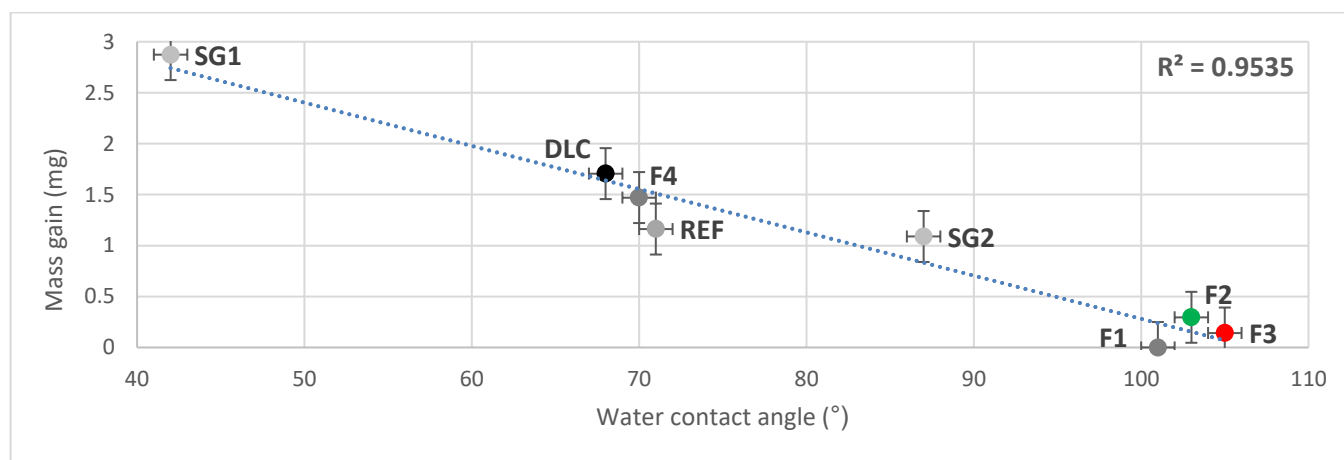


**Figure 24** Water contact angle vs. mass gain – PbS multiphase conditions

Figure 25 (i-ii) shows a post-experimental emulsion of oil, PbS particles and water, formed through vigorous shaking (i); with breaking of the oil and Pickering emulsion after 40 seconds; and significant migration of PbS particles from the water phase to the interface after a period of approximately 220 seconds (ii). Figure 25 (iii) displays an optical microscope image of the PbS stabilized o/w Pickering emulsion at 20x magnification, where stabilised oil droplets range from 100-700  $\mu\text{m}$  in diameter.

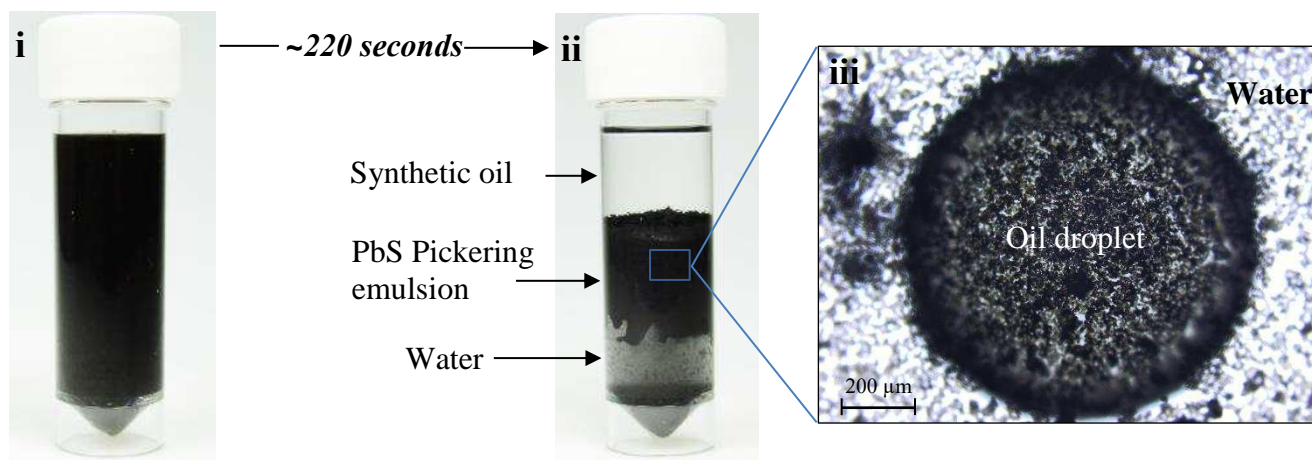
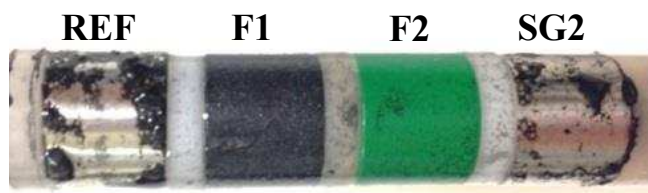


**Figure 25** Oil, emulsion and brine phase separation: i) PbS emulsion after shaking; ii) separation of oil phase (40 seconds) and significant migration of PbS particles from water to o/w interface after approximately 220 seconds; iii) Optical microscope image of PbS stabilized oil droplet within emulsion (x20 mag)

Hydrophobic fluoropolymer surfaces are wet by the oil present within the turbulent o/w emulsion, preventing the impaction of oil droplets encased by partially-wetted PbS particles. From Figure 25 it can be seen that the PbS particles stabilized within the o/w Pickering emulsion are highly oleophobic. The faster separation speed of the PbS micro-emulsion from the oil phase indicates that PbS particles display hydrophilicity, as the oil-water contact angle ( $\theta_{ow}$ ) is less than  $90^\circ$ .

#### 4.7. Pre-precipitated PbS adhesion

Adhesion was predicted to be the sole mechanism by which PbS scale deposited on to surfaces within the scaling system, due to the spontaneous homogenous precipitation of scale within the bulk phase. Figure 26 and Table 9 show the degree of PbS deposition through mass gain measurements when new anti-fouling surfaces were inserted into the multiphase system post-experiment, and the test repeated in brine and oil with pre-precipitated PbS.



10 **Figure 26** Photographs of samples – PbS  
11 multiphase conditions (pre-precipitated)  
12  
13  
14  
15

16  
17  
18  
19  
20  
21  
22  
23  
24  
25  
26  
27

Coating	Mass gain (mg)	Water contact angle (°)
REF	0.6±0.05	71
F1	0.1±0.03	101
F2	0.2±0.04	103
SG2	0.6±0.07	87

28 **Table 9** Coating PbS mass gain – PbS multiphase  
29 conditions (pre-precipitated)  
30  
31  
32  
33

34  
35 Deposition of PbS on anti-fouling surfaces in a pre-precipitated system follows a similar trend to that  
36 seen during initial multiphase scaling tests, with wettability characteristics of the coatings influencing  
37 degree of scale build-up. Upon comparison of Figure 21 and Figure 26 however, it can be seen there was  
38 generally less deposition on all surfaces in pre-precipitated systems. This may be explained through a  
39 significant proportion of existing PbS scale precipitated in the initial test being deposited onto the reaction  
40 vessel and initial samples during the first experiment. Consequently, there is less PbS within the system  
41 after a second test is carried out in a pre-precipitated system, reducing the likelihood of scale particles  
42 contacting the anti-fouling surface and forming deposits.  
43  
44  
45  
46  
47  
48  
49  
50  
51  
52  
53  
54  
55  
56  
57  
58  
59  
60

#### 4.8. PbS Pickering emulsion rheology

Rheology measurements showed that breaking of the PbS Pickering emulsion occurred at very low shear values of approximately 0.1 Pa (Figure 27), whilst the shear wall stress at the interface of anti-fouling samples was calculated to be 0.17 Pa (Table 8).

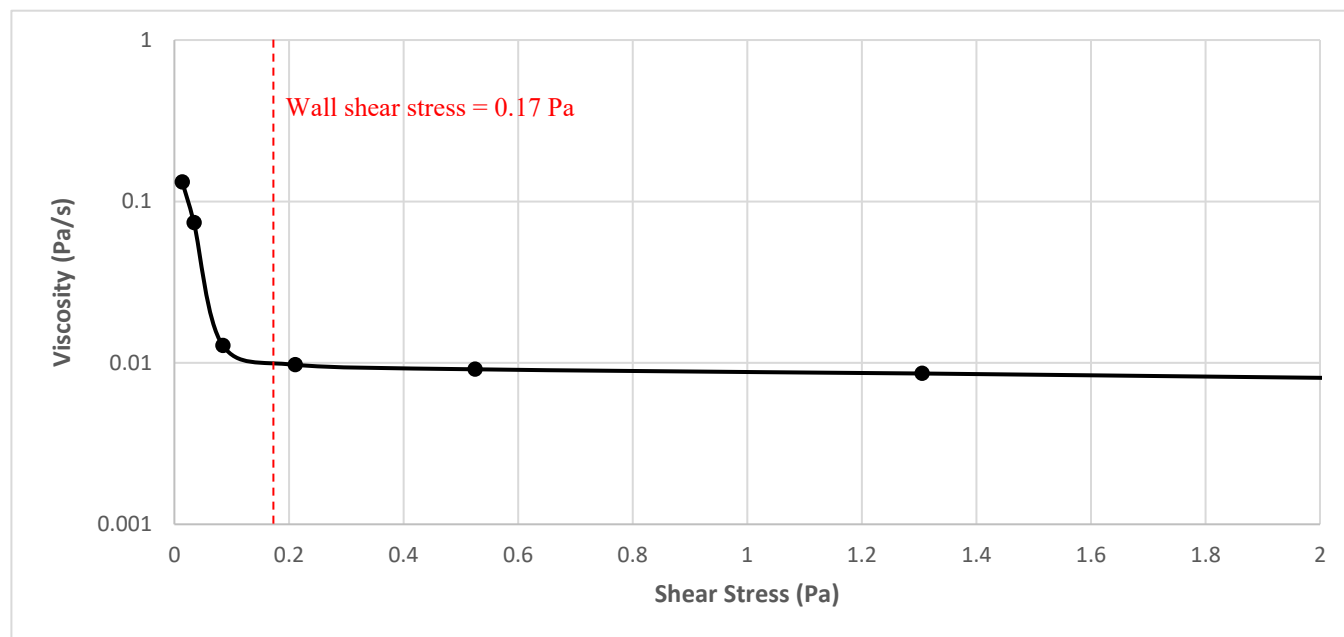


**Figure 27** Shear stress vs. viscosity of o/w PbS Pickering emulsion at shear values of 0-2 Pa

From the hydrodynamic conditions propagated by rotation of the cylindrical coupons in solution (Table 8), it can be seen that the PbS Pickering emulsion underwent a sharp reduction in viscosity from approximately 0.13 Pa/s at 0.014 Pa shear stress, to 0.012 Pa/s at 0.1 Pa shear stress, before reaching relative equilibrium and exhibiting Newtonian behavior. This drop in viscosity is indicative of emulsion droplet breaking, where large shear stresses can prompt oil droplets within the emulsion to rupture and destabilize<sup>36</sup>.

## 5. DISCUSSION

Hydrophobic fluoropolymer surfaces have the ability to drastically reduce deposition in multiphase systems where homogeneously precipitated scales have hydrophilic properties. This is caused by oil wetting of hydrophobic surfaces and consequent formation of a protective barrier, shielding from impaction and adhesion of crystals that are partially or fully wetted to the bulk brine phase<sup>37</sup>.

Though the kinetics of salt precipitation may vary based on species and external conditions<sup>38</sup>, critical nucleus size of a given compound in solution generally decreases as a function of increasing critical SR<sup>39</sup>. When SR<sub>initial</sub> is sufficiently high to prompt instantaneous nucleation in the bulk aqueous phase, depositional behavior by way of adhesion can be accurately predicted based on the wettability of foreign surfaces. As such, a relationship can be drawn between the SR<sub>initial</sub> of a mineral salt, and the strength of the ‘water contact angle vs. mass gain’ negative correlation, in a brine to oil ratio of 95:5 (v/v), as seen in Table 10.

Salt	SR <sub>initial</sub>	R <sup>2</sup> value (negative)
CaCO <sub>3</sub>	76	0.19
BaSO <sub>4</sub>	1888	0.42
PbS	2.8x10 <sup>22</sup>	0.95

**Table 10** SR<sub>initial</sub> and R<sup>2</sup> values in multiphase

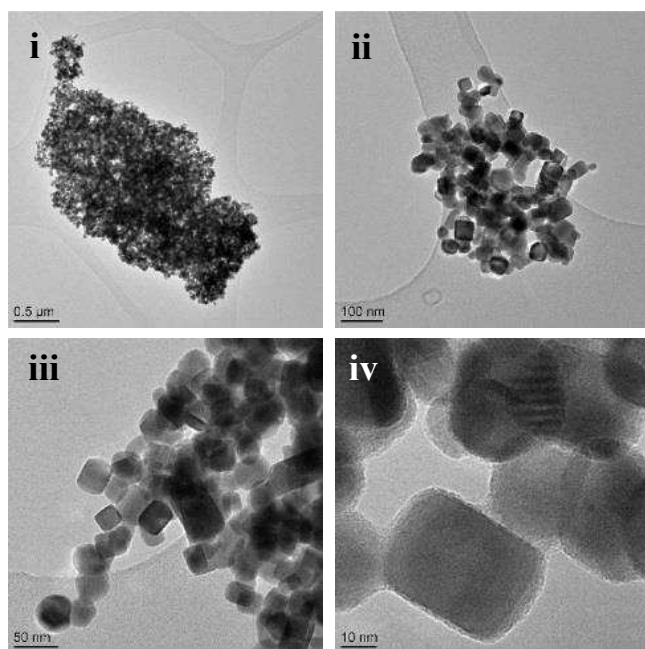
### 5.1. Scale nucleation mechanisms

Due to the very low solubility product of PbS in water ( $K_{sp} = 4 \times 10^{-28} \text{ mol}^2 \text{ dm}^{-6}$ ), the SR<sub>initial</sub> reaches a value of approximately  $2.8 \times 10^{22}$  when Ionic Activity Product (IAP) concentrations of reactants typically seen in oilfield systems are applied experimentally<sup>40</sup>. However, conventional scales are far more soluble than PbS in water, with a  $K_{sp}$  value of  $3.8 \times 10^{-9} \text{ mol}^2 \text{ dm}^{-6}$  and  $1.1 \times 10^{-10} \text{ mol}^2 \text{ dm}^{-6}$  for CaCO<sub>3</sub> and BaSO<sub>4</sub> respectively<sup>41, 42</sup>. As the SR<sub>initial</sub> of CaCO<sub>3</sub> and BaSO<sub>4</sub> are approximately 19 orders of magnitude lower

1 than PbS given an identical IAP, the thermodynamic driving force for nucleation to occur is significantly  
2 reduced compared to PbS. In systems prone to  $\text{CaCO}_3$  and  $\text{BaSO}_4$  scaling, the presence of a foreign surface  
3 within a system is likely to induce nucleation at degrees of super-cooling lower than those required for  
4 homogeneous nucleation, resulting in increased heterogeneous nucleation <sup>34</sup>. In both conventional and  
5 sulfide scaling systems, crystal growth after nucleation is likely to occur by way of Ostwald ripening  
6 mechanism <sup>34, 43</sup>.  
7  
8  
9  
10  
11  
12  
13

## 17 5.2. PbS Characterization

18 Transmission Electron Microscopy (TEM) imaging revealed the size and morphology of precipitated  
19 nano-sized PbS particles, as presented in Figure 28 (i-iv).  
20  
21  
22  
23  
24  
25



48 **Figure 28** TEM images of precipitated PbS  
49 crystals – single phase  
50  
51  
52  
53  
54

55 Agglomerates of PbS particles within a single phase system formed clusters of approximately 0.5-5  
56 microns in diameter, visible in Figure 28 (i) and (ii) respectively. Due to the nanometric size of the  
57  
58  
59  
60

1 particles, agglomeration occurs through minimization of surface energy, as well as attractive Van-der-  
2  
3 Waals and electrostatic interactions between particles of a similar type <sup>28</sup>.  
4

5 Individual crystals of PbS precipitated in the homogeneous single phase are of cubic morphology and  
6  
7 range from 30-60 nm in diameter, as represented in Figure 28 (iii and iv). The PbS particles formed are  
8  
9 therefore within the range of 20-100nm, as reported by Andritsos and Karabelas for spontaneous  
10  
11 nucleation <sup>16</sup>. The very high  $SR_{initial}$  of PbS in the experimental system ( $SR=2.8 \times 10^{22}$ ) likely results in  
12  
13 different growth velocities at crystal faces. This leads to curving of crystal edges and the formation of  
14  
15 rounded rectangle to spherically shaped crystals, in contrast to  $CaCO_3$  crystals characterized by sharp,  
16  
17 clearly defined edges due to significantly slower growth rates <sup>44</sup>.  
18  
19  
20  
21  
22  
23

### 24 **5.3. Particle behavior and emulsion stability**

25  
26 Free energy of adsorption is strongest when particle contact angle at the interface is  $90^\circ$ , with larger  
27  
28 particles having higher stability as a result of increased contact area with oil and water phases either side  
29  
30 of the interface, as shown by capillary rise experiments carried out by Kirchberg et al. <sup>27</sup> on iron silicon  
31  
32 (FeSi) and magnetite ( $Fe_3O_4$ ). Consequently, the larger calcite crystal was expected to have higher stability  
33  
34 at the o/w interface than PbS nanoparticles given ideal partial wetting. However, wetting of particles in  
35  
36 both the oil and water phase has a significant bearing on interfacial stability, with too substantial a disparity  
37  
38 between respective contact angles leading to total wetting and dispersion within one phase <sup>24</sup>. From  
39  
40 literature, the water contact angle of a calcite particle is  $6^\circ$  <sup>45</sup>, with oil contact angle on cleaved calcite  $81^\circ$   
41  
42 in distilled water and  $130^\circ$  in 1M NaCl <sup>46</sup>. High hydrophilicity and low oleophilicity of calcite particles  
43  
44 therefore leads to complete dispersion within the aqueous phase, with a negligible amount of crystals  
45  
46  
47  
48  
49  
50  
51 stabilized at the oil/water interface.

52  
53 Intermediate hydrophobicity of PbS nanoparticles lead to formation of a Pickering emulsion stabilized  
54  
55 between excess oil and water phases, creating a 'Winsor – type III' emulsion, as seen in Figure 25 (ii) <sup>47</sup>.  
56  
57 Mechanical strength of droplets is derived from aggregation of solid particles at the surface, with partially-  
58  
59  
60

wetted solid particles held together in a layer at the oil/water interface by attractive interactions such as capillary forces, with both intermolecular dispersion and electrostatic repulsion further influencing wetting and stability<sup>24</sup>.

Recent research by Kim et al.<sup>26</sup> has established the importance of the size of synthesized silicon particles, ranging from 5 nm to 80 nm, on Pickering emulsion stability and phase distribution in ‘Winsor – type III’ emulsions. The phase ratio of the ‘stabilized emulsion’ to oil and brine can be seen to decrease as particle size increases (Figure 29).

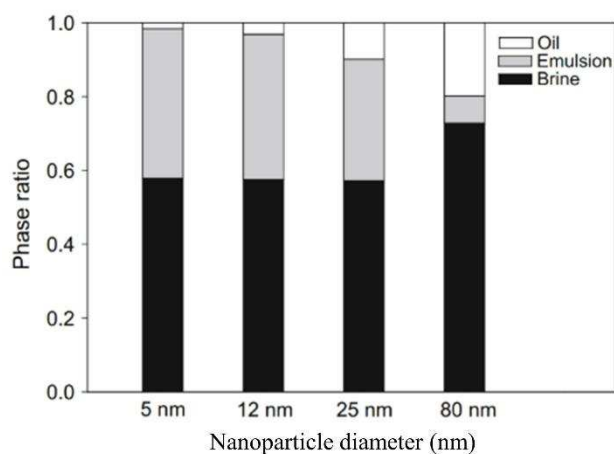


**Figure 29** Excess oil, emulsion, and excess brine phase separation (from Kim et al.<sup>26</sup>)

As PbS particles are thermodynamically stable between 25 and 80nm (Figure 29), a persistent Pickering emulsion is formed within the reacting multiphase system (Figure 25 (ii)). As the oil phase is not completely emulsified, the separated oil enveloped hydrophobic surfaces present within the system, consequently creating a barrier that prevented emulsion sticking.

Single phase PbS deposition was driven by van der Waals (VDW), electrostatic double layer (EDL) interactions and gravity. It has been shown that increased flow velocity ultimately reduces particle deposition, where particles are readily swept away resulting in reduced likelihood of contact with the

1 coating surface<sup>48</sup>. Whilst the effect of surface forces is more apparent for smaller particles and deposition  
2 rate consequentially higher, the agglomeration of nanometric PbS (Figure 28(i)) to clusters approximately  
3 3 microns in diameter significantly reduces surface to volume ratio. Agglomeration can be explained by a  
4 measured PbS particle zeta potential of -8 mV at pH 5.2, where weak electrostatic repulsion force leads  
5 to dominance of VDW attraction between PbS nanoparticles. As such, deposition upon all anti-fouling  
6 surfaces at a Reynolds number of 3374 is negligible, as seen in Figure 16.  
7  
8  
9  
10  
11  
12  
13

14 In a PbS forming multiphase system, rheological measurements (Figure 27) showed that the o/w PbS  
15 Pickering emulsion breaks when exposed to shear stresses of approximately 0.1 Pa. Shear stress of 0.17  
16 Pa at the coating interface therefore results in oil droplet destabilisation and rupture, whereby stabilising  
17 PbS particles from the o/w interface are splayed across hydrophilic coatings after droplet impaction and  
18 breaking. It is probable that once a layer of PbS scale has been initially deposited, the anti-fouling  
19 properties of the coating are negated, with Figure 21 (SG1) showing the adhesion of intact PbS stabilised  
20 oil droplets upon the surface.  
21  
22  
23  
24  
25  
26  
27  
28  
29  
30  
31  
32  
33

#### 34 **5.4. Industrial ramifications**

35  
36 Metal sulfide scales have been reported to deposit with increased severity towards the top of the production  
37 tubing as opposed to areas around the wellbore, where carbonate and sulfate scales are dominant. General  
38 consensus within the oil and gas industry is that, as with conventional scales, precipitation of PbS is a  
39 direct result of temperature and pressure reduction as produced flow reaches the upper part of the well,  
40 triggering the liberation of CO<sub>2</sub> and a consequent pH increase<sup>8</sup>.  
41  
42  
43  
44  
45  
46  
47

48 Though metal sulfide precipitation is strongly influenced by the temperature and pH of a system<sup>6</sup>, it is  
49 unlikely that even the severest of downhole conditions would be sufficient to solubilize PbS. Clever and  
50 Johnston state that the  $K_{sp}$  of PbS is  $4.4 \times 10^{-21} \text{ mol}^2 \text{ dm}^{-6}$  at 473K, giving an SR of  $5.13 \times 10^{13}$  at Pb<sup>2+</sup> cation  
51 concentrations as low as 50mg/L, typical of levels reported in the formation water of fields prone to metal  
52 sulfide scaling<sup>8, 49</sup>. Additionally, the deposition of PbS is driven by heterogeneous nucleation at  
53  
54  
55  
56  
57  
58  
59  
60

1 approximately pH 1.7, with spontaneous precipitation occurring under pH conditions any higher <sup>35</sup>.  
2  
3 However, pH values of produced water cited in case studies of HT/HP sour reservoirs typically lie between  
4  
5 6 and 7 <sup>50</sup>, falling as low as pH 5 under the most extreme of conditions <sup>51, 52</sup>.  
6

7 The kinetic stability of o/w emulsions is drastically reduced by increased temperature, whereby the  
8  
9 viscosity of the oil, water and properties of interfacial films are affected. Sharma et al. <sup>53</sup> showed that  
10  
11 oil/water interfacial tension (IFT) of emulsions stabilized by 1% SiO<sub>2</sub> nanoparticles underwent a sharp  
12  
13 decrease at temperatures between 350 and 360 K, with droplet size increasing and the emulsion loosening  
14  
15 and breaking as a result. In practicality, producing oilfield wells contain high levels of total dissolved  
16  
17 solids (TDS), as well as surfactants, polymeric inhibitors, and other colloidal particles e.g. clay fines, that  
18  
19 can all contribute to emulsion stabilisation. Furthermore, Sharma et al. <sup>53</sup> showed that 1 wt% SiO<sub>2</sub>  
20  
21 nanoparticle Pickering emulsions containing 0.22 wt% surfactant and 1 wt% NaCl are stable and able to  
22  
23 withstand droplet agglomeration up to 379K. Whilst bottom-hole temperature (BHT) may be in the range  
24  
25 of 423-478 K in a HT/HP system, it is conceivable that cooling of the produced oil and water stream to  
26  
27 approximately 379 K may result in emulsion stabilisation. The temperature and location at which emulsion  
28  
29 stabilisation occurs will be based on a multitude of variables, including colloidal characteristics, salt  
30  
31 concentration, surfactant and polymer concentration and the temperature profile of the well in question <sup>54</sup>.  
32  
33 It is entirely feasible that PbS scale homogeneously precipitated in the wellbore deposits on surfaces and  
34  
35 equipment towards the upper part of the production line as a result of the increased adhesion and deposition  
36  
37 tendency of PbS particles in a stabilized Pickering emulsion. As temperature decreases up the production  
38  
39 tubing towards the surface, loose, un-adhesive PbS agglomerates are adsorbed at the oil/water interface,  
40  
41 with the impacting o/w emulsion droplets contributing to scale build-up on surfaces under a turbulent flow  
42  
43 regime.  
44  
45  
46  
47  
48  
49  
50

51  
52 Calculation of parameters such as particle size and wettability, temperature, phase viscosity, pH, TDS  
53  
54 downhole and temperature profile of the well may lead to the ability to predict the severity and location  
55  
56 of sulfide deposits given development of a suitable scaling model.  
57  
58  
59  
60

## 6. CONCLUSIONS

1  
2  
3 The role of a light oil phase with regards to deposition of in turbulent systems is significant. In carbonate  
4  
5 systems, where heterogeneous nucleation is the predominant deposition mechanism, the influence of an  
6  
7 oil phase is diminished. As homogeneous nucleation becomes prevalent due to heightened  $SR_{initial}$  of  
8  
9 forming salts, both the influence of an enveloping oil layer and transport of partially-wetted scale particles  
10  
11 become more substantial.

14  
15 PbS scale is partially-wetted at the oil/water interface, in part due to the nanometric particle size as a  
16  
17 result of spontaneous precipitation, leading to limited hydrophilicity, and consequently forming a stable  
18  
19 o/w Pickering emulsion. Adsorption of partially-wetted PbS nanoparticles at the o/w interface of stabilized  
20  
21 oil droplets within a turbulent multiphase regime prompts impaction upon surfaces, resulting in deposition.  
22  
23 In single phase systems, loose agglomerates of PbS acting through turbulent and gravitational deposition  
24  
25 show negligible deposition on all anti-fouling surfaces due to lack of adherence. The wettability of anti-  
26  
27 fouling coatings correlate increasingly strongly with mass gain as the ratio of scale precipitated  
28  
29 homogeneously within a multiphase system increases. Hydrophobic fluoropolymer coatings see negligible  
30  
31 deposition on their surfaces in highly supersaturated multiphase systems e.g. PbS, as a result of an  
32  
33 enveloping oil layer protecting from impaction of scale particle encased oil droplets upon their surface.  
34  
35 PbS scaling experiments within pre-precipitated brine showed that adhesion is the sole mechanism of scale  
36  
37 deposition upon anti-fouling surfaces.

42  
43 From approximate prediction of the scaling tendency of PbS in HT/HP wells at cation concentrations  
44  
45 comparable to those in the field, it is highly probable that precipitation occurs instantaneously within the  
46  
47 formation as soon as  $H_2S$  diffuses into the aqueous phase. Reported deposition of PbS in the upper regions  
48  
49 of the producing well indicate that, rather than heterogeneously precipitating as a result of SR increase  
50  
51 due to reduced temperature and pressure, PbS Pickering emulsions are stabilized as a result of these  
52  
53 physical changes, leading to adhesion. It is conceivable that, given a sufficient cation concentration and  
54  
55

1 SR, deposition of other sparingly soluble inorganic scales such as ZnS can be explained via a similar  
2 mechanism.  
3  
4  
5  
6  
7

## 8 ASSOCIATED CONTENT

### 9 Supporting information

10 The supporting information is available free of charge on the ACS Publications website at DOI:

11  
12 Bjerren plots showing the effect of pH on H<sub>2</sub>CO<sub>3</sub> and H<sub>2</sub>S species dissociation (Figures S1 and  
13  
14 S2), XRD Spectra of calcite formed in single phase under ambient conditions (Figure S3),  
15  
16 Experimental scaling rig (Figure 4)  
17  
18  
19  
20  
21  
22  
23  
24

## 25 AUTHOR INFORMATION

### 26 Corresponding Author

27 \*Tel. +447772076496. E-mail: [pm09wk@leeds.ac.uk](mailto:pm09wk@leeds.ac.uk)  
28  
29  
30  
31

### 32 ORCID

33 William Keogh: 0000-0003-3676-8129  
34  
35

### 36 Notes

37 The authors declare no competing financial interest  
38  
39  
40  
41  
42  
43

## 44 ACKNOWLEDGEMENTS

45 The authors acknowledge the funding and support from the Leeds University ASSESS consortium. We  
46  
47 also thank the financial support of the Leverhulme Trust Research Grant ECF-2016-204  
48  
49  
50  
51  
52  
53  
54  
55  
56  
57  
58  
59  
60

## NOMENCLATURE

1  
2  
3 BaSO<sub>4</sub> = barium sulfate  
4 BHT = bottom-hole temperature  
5 CaCO<sub>3</sub> = calcium carbonate  
6 CO<sub>2</sub> = carbon dioxide  
7 EDX = energy-dispersive x-ray spectroscopy  
8  
9 FW = formation water  
10 H<sub>2</sub>S = hydrogen sulfide  
11 HT/HP = high temperature/high pressure  
12 IAP = ion activity product  
13 IFT = interfacial tension  
14 K = kelvin  
15 K<sub>sp</sub> = solubility product  
16 MVT = Mississippi valley type  
17 N<sub>2</sub> = nitrogen  
18 Na<sub>2</sub>S = sodium sulfide  
19 NaCl = sodium chloride  
20 o/w = oil/water  
21 PbS = lead sulfide  
22 ppm = parts-per-million  
23 RCE = rotating cylinder electrode  
24 SEM = scanning electron microscopy  
25 SR = saturation ratio  
26 SRB = sulfate reducing bacteria  
27 SrSO<sub>4</sub> = strontium sulfate  
28 SW = seawater  
29 TDS = total dissolved solids  
30 TEM = transmission electron microscopy  
31 VDW = van der Waals  
32 XRD = x-ray diffraction  
33 ZnS = zinc sulfide  
34  
35  
36  
37  
38  
39  
40  
41  
42  
43  
44  
45  
46  
47

## REFERENCES

1. Bukuaghagin, O.; Sanni, O.; Kapur, N.; Huggan, M.; Neville, A.; Charpentier, T., Kinetics study of barium sulphate surface scaling and inhibition with a once-through flow system. *Journal of Petroleum Science and Engineering* **2016**, 147, 699-706.
2. Sanni, O.; Charpentier, T.; Kapur, N.; Neville, A. In Study of surface deposition and bulk scaling kinetics in oilfield conditions using an in-situ flow rig, NACE-International Corrosion Conference Series, 2015; Leeds: **2015**.

3. Vazirian, M. M.; Charpentier, T. T. J.; Neville, A.; Alvim, F. B.; de Oliveira Penna, M., Assessing Surface Engineering Solutions for Oilfield Scale; Correlating Laboratory Tests to Field Trials. In Society of Petroleum Engineers: **2016**.
4. Okocha, C.; Sorbie, K. In Scale Prediction for Iron, Zinc and Lead Sulphides and Its Relation to Scale Test Design, CORROSION 2014, 2014; NACE International: **2014**.
5. Chen, T.; Chen, P.; Montgomerie, H.; Hagen, T. H.; Jeffrey, C. In Development of Test Method and Inhibitors for Lead Sulfide, SPE International Conference on Oilfield Scale, 2010; Society of Petroleum Engineers: **2010**.
6. Al-Harbi, B. G.; Graham, A. J.; Sorbie, K. S., Zinc and Lead Interactions in Combined Sulphide Scales. In Society of Petroleum Engineers: **2017**.
7. Okocha, C.; Sorbie, K. S.; Hurtevent, C.; Baraka-Lokmane, S.; Rossiter, M., Sulphide Scale (PbS/ZnS) Formation and Inhibition Tests for a Gas Condensate Field with Severe Scaling Conditions. In SPE International, Society of Petroleum Engineers: Aberdeen, United Kingdom, **2014**.
8. Baraka-Lokmane, S.; Hurtevent, C.; Rossiter, M.; Bryce, F.; Lepoivre, F.; Marais, A.; Tillement, O.; Simpson, C.; Graham, G. In Design and Performance of Novel Sulphide Nanoparticle Scale Inhibitors for North Sea HP/HT Fields, SPE International Oilfield Scale Conference and Exhibition, 2016; Society of Petroleum Engineers: **2016**.
9. Bellarby, J., Well completion design. Elsevier: **2009**; Vol. 56.
10. Jordan, M.; Mackin, K.; Johnston, C.; Feasey, N. In Control of hydrogen sulphide scavenger induced scale and the associated challenge of sulphide scale formation within a North Sea high temperature/high salinity fields production wells. Laboratory evaluation to field application, SPE International Symposium on Oilfield Scale, 2004; Society of Petroleum Engineers: **2004**.
11. Leach, D. L.; Taylor, R. D.; Fey, D. L.; Diehl, S. F.; Saltus, R. W. A deposit model for Mississippi Valley-Type lead-zinc ores: Chapter A in Mineral deposit models for resource assessment; 2328-0328; US Geological Survey: 2010.
12. Kelland, M. A., Production Chemicals for the Oil and Gas Industry, Second Edition. Taylor & Francis: **2014**.
13. Collins, I.; Jordan, M. In Occurance, Prediction And Prevention Of Zinc Sulfide Scale Within Gulf Coast And North Sea High Temperature/High Salinity Production Wells, International Symposium on Oilfield Scale, 2001; Society of Petroleum Engineers: **2001**.
14. Eden, B.; Laycock, P. J.; Fielder, M., Oilfield reservoir souring. HSE Books Suffolk, England: 1993.
15. Dong, L.; Chu, Y.; Zhuo, Y.; Zhang, W., Two-minute synthesis of PbS nanocubes with high yield and good dispersibility at room temperature. Nanotechnology **2009**, 20, (12), 125301.
16. Andritsos, N.; Karabelas, A., Sulfide scale formation and control: the case of lead sulfide. Geothermics **1991**, 20, (5), 343-353.
17. Okocha, C.; Sorbie, K.; Boak, L., Novel Inhibition Mechanism for Sulfide Scales. Paper SPE 112538 presented at the SPE International Symposium and Exhibition on Formation Damage Control, Lafayette, Louisiana, USA, 13–15 February. In **2008**.
18. Lopez, T. H.; Yuan, M.; Williamson, D. A.; Przybylinski, J. L. In Comparing efficacy of scale inhibitors for inhibition of zinc sulfide and lead sulfide scales, SPE International Symposium on Oilfield Scale, 2005; Society of Petroleum Engineers: **2005**.
19. Cheong, W.; Gaskell, P.; Neville, A., Substrate effect on surface adhesion/crystallisation of calcium carbonate. Journal of Crystal Growth **2013**, 363, 7-21.
20. Vazirian, M. M.; Charpentier, T. V. J.; de Oliveira Penna, M.; Neville, A., Surface inorganic scale formation in oil and gas industry: As adhesion and deposition processes. Journal of Petroleum Science and Engineering **2016**, 137, 22-32.
21. Charpentier, T.; Neville, A.; Baraka-Lokmane, S.; Hurtevent, C.; Ordonez-Varela, J.; Nielsen, F. M.; Eroini, V.; Olsen, J.; Ellingsen, J.; Bache, Ø. In Evaluation of Anti-fouling Surfaces for Prevention of Mineral Scaling in Sub-surface Safety Valves, SPE International Oilfield Scale Conference and Exhibition, 2014; Society of Petroleum Engineers: 2014.
22. Bukuaghagin, O.; Neville, A.; Charpentier, T. V. In Scale Formation in Multiphase Conditions, Proceedings of the Oil Field Chemistry Symposium, Gielo, 2015; **2015**.
23. Böker, A.; He, J.; Emrick, T.; Russell, T. P., Self-assembly of nanoparticles at interfaces. Soft Matter **2007**, 3, (10), 1231-1248.

- 1  
2  
3  
4  
5  
6  
7  
8  
9  
10  
11  
12  
13  
14  
15  
16  
17  
18  
19  
20  
21  
22  
23  
24  
25  
26  
27  
28  
29  
30  
31  
32  
33  
34  
35  
36  
37  
38  
39  
40  
41  
42  
43  
44  
45  
46  
47  
48  
49  
50  
51  
52  
53  
54  
55  
56  
57  
58  
59  
60
24. Chevalier, Y.; Bolzinger, M.-A., Emulsions stabilized with solid nanoparticles: Pickering emulsions. *Colloids and Surfaces A: Physicochemical and Engineering Aspects* **2013**, 439, 23-34.
  25. Bebie, J.; Schoonen, M. A.; Fuhrmann, M.; Strongin, D. R., Surface charge development on transition metal sulfides: an electrokinetic study. *Geochimica et Cosmochimica Acta* **1998**, 62, (4), 633-642.
  26. Kim, I.; Worthen, A. J.; Johnston, K. P.; DiCarlo, D. A.; Huh, C., Size-dependent properties of silica nanoparticles for Pickering stabilization of emulsions and foams. *Journal of Nanoparticle Research* **2016**, 18, (4), 82.
  27. Kirchberg, S.; Abdin, Y.; Ziegmann, G., Influence of particle shape and size on the wetting behavior of soft magnetic micropowders. *Powder Technology* **2011**, 207, (1-3), 311-317.
  28. Amjad, Z.; Demadis, K. D., *Mineral Scales and Deposits: Scientific and Technological Approaches*. Elsevier: **2015**.
  29. Palomar-Pardave, M.; Gonzales, I.; Romero-Romo, M.; Oropez, T.; Palomar-Pardave, M., MES 23: Electrochemistry, Nanotechnology, and Biomaterials. In *Electrochemical Society: Pennington, NJ, USA: 2008*.
  30. Venkateshwaran, V.; Vembanur, S.; Garde, S., Water-mediated ion-ion interactions are enhanced at the water vapor-liquid interface. *Proceedings of the National Academy of Sciences* **2014**, 111, (24), 8729-8734.
  31. Chevalier, N. R.; Guenoun, P., Surface Tension Drives the Orientation of Crystals at the Air-Water Interface. *The Journal of Physical Chemistry Letters* **2016**, 7, (14), 2809-2813.
  32. Forsyth, C.; Mulheran, P. A.; Forsyth, C.; Haw, M. D.; Burns, I. S.; Sefcik, J., Influence of Controlled Fluid Shear on Nucleation Rates in Glycine Aqueous Solutions. *Crystal Growth & Design* **2015**, 15, (1), 94-102.
  33. Agrawal, S. G. *Evaporative crystallization of alpha-lactose monohydrate: a thesis presented in partial fulfilment of the requirements for the degree of Doctor of Philosophy in Chemical Engineering at Massey University, Manawatu, New Zealand. Massey University, 2012*.
  34. Mullin, J. W., *Crystallization*. Butterworth-Heinemann: **2001**.
  35. Andritsos, N.; Karabelas, A., Crystallization and deposit formation of lead sulfide from aqueous solutions: II. Morphology of the deposits. *Journal of colloid and interface science* **1991**, 145, (1), 170-181.
  36. Whitby, C. P.; Krebsz, M., Coalescence in concentrated Pickering emulsions under shear. *Soft matter* **2014**, 10, (27), 4848-4854.
  37. Sousa, M.; Barbosa, G.; Signorelli, F.; Bertran, C., Anti-scaling properties of a SLIPS material prepared by silicon oil infusion in porous polyaniline obtained by electropolymerization. *Surface and Coatings Technology* **2017**.
  38. Nancollas, G.; Reddy, M., The kinetics of crystallization of scale-forming minerals. *Society of Petroleum Engineers Journal* **1974**, 14, (02), 117-126.
  39. Brus, D.; Ždímal, V.; Smolík, J., Homogeneous nucleation rate measurements in supersaturated water vapor. *The Journal of chemical physics* **2008**, 129, (17), 174501.
  40. Kong, Y.; Chen, J.; Fang, H.; Heath, G.; Wo, Y.; Wang, W.; Li, Y.; Guo, Y.; Evans, S. D.; Chen, S., Highly Fluorescent Ribonuclease-A-Encapsulated Lead Sulfide Quantum Dots for Ultrasensitive Fluorescence in Vivo Imaging in the Second Near-Infrared Window. *Chemistry of Materials* **2016**, 28, (9), 3041-3050.
  41. Rattanasak, U.; Pankhet, K.; Chindaprasirt, P., Effect of chemical admixtures on properties of high-calcium fly ash geopolymer. *International Journal of Minerals, Metallurgy, and Materials* **2011**, 18, (3), 364-369.
  42. Guyette, R. P.; Cutter, B. E., Barium and manganese trends in tree-rings as monitors of sulfur deposition. *Water, Air, & Soil Pollution* **1994**, 73, (1), 213-223.
  43. Lignos, I.; Stavrakis, S.; Kilaj, A.; deMello, A. J., Millisecond-Timescale Monitoring of PbS Nanoparticle Nucleation and Growth Using Droplet-Based Microfluidics. *Small* **2015**, 11, (32), 4009-4017.
  44. Judat, B.; Kind, M., Morphology and internal structure of barium sulfate—derivation of a new growth mechanism. *Journal of Colloid and Interface Science* **2004**, 269, (2), 341-353.
  45. KOWALCZUK, P. B.; AKKAYA, C.; ERGUN, M.; JANICKI, M. J.; SAHBAZ, O.; DRZYMALA, J., WATER CONTACT ANGLE ON CORRESPONDING SURFACES OF FRESHLY FRACTURED FLUORITE, CALCITE AND MICA. *Physicochem. Probl. Miner. Process* **2017**, 53, (1), 192-201.
  46. Aslan, S.; Fathi Najafabadi, N.; Firoozabadi, A., Non-monotonicity of the Contact Angle from NaCl and MgCl<sub>2</sub> Concentrations in Two Petroleum Fluids on Atomistically Smooth Surfaces. *Energy & Fuels* **2016**, 30, (4), 2858-2864.
  47. Strey, R., Microemulsion microstructure and interfacial curvature. *Colloid and Polymer Science* **1994**, 272, (8), 1005-1019.

- 1 48. Unni, H.; Yang, C., Kinetics of colloidal particle deposition to a solid surface from pressure driven  
2 microchannel flows. *The Canadian Journal of Chemical Engineering* **2007**, 85, (5), 609-616.
- 3 49. Clever, H. L.; Johnston, F. J., The solubility of some sparingly soluble lead salts: an evaluation of the  
4 solubility in water and aqueous electrolyte solution. *Journal of Physical and Chemical Reference Data* **1980**, 9,  
5 (3), 751-784.
- 6 50. Verri, G.; Sorbie, K. S.; Singleton, M. A.; Silva, D.; Hinrichsen, C.; Wang, Q.; Chang, F. F., A New  
7 Approach to Combined Sulphide and Carbonate Scale Predictions Applied to Different Field Scenarios. In  
8 *Society of Petroleum Engineers*: **2017**.
- 9 51. Li, Y.; She, C.; Liu, N.; Zhang, H.; Zhang, L.; Zhu, D., Completion difficulties of HTHP and high-  
10 flowrate sour gas wells in the Longwangmiao Fm gas reservoir, Sichuan Basin, and corresponding  
11 countermeasures. *Natural Gas Industry B* **2016**.
- 12 52. Ramachandran, S.; Al-Muntasheri, G.; Leal, J.; Wang, Q. In *Corrosion and Scale Formation in High*  
13 *Temperature Sour Gas Wells: Chemistry and Field Practice*, SPE International Symposium on Oilfield  
14 *Chemistry*, 2015; Society of Petroleum Engineers: **2015**.
- 15 53. Sharma, T.; Kumar, G. S.; Chon, B. H.; Sangwai, J. S., Thermal stability of oil-in-water Pickering  
16 emulsion in the presence of nanoparticle, surfactant, and polymer. *Journal of Industrial and Engineering*  
17 *Chemistry* **2015**, 22, 324-334.
- 18 54. Bruijn, G.; Skeates, C.; Greenaway, R.; Harrison, D.; Parris, M.; James, S.; Mueller, F.; Ray, S.; Riding,  
19 M.; Temple, L., High-Pressure. High-Temperature Technologies []. *Journal of Petrology* **2008**.
- 20  
21  
22  
23  
24  
25  
26  
27  
28  
29  
30  
31  
32  
33  
34  
35  
36  
37  
38  
39  
40  
41  
42  
43  
44  
45  
46  
47  
48  
49  
50  
51  
52  
53  
54  
55  
56  
57  
58  
59  
60